THE LARGE ANGLE SPECTROSCOPIC CORONAGRAPH (LASCO)

Visible Light Coronal Imaging And Spectroscopy

G. E. BRUECKNER, R. A. HOWARD, M. J. KOOMEN, C. M. KORENDYKE, D. J. MICHELS, J. D. MOSES, D. G. SOCKER and K. P. DERE
E. O. Hulburt Center for Space Research, Naval Research Laboratory Washington D.C., 20375-5320 USA

P. L. LAMY, A. LLEBARIA, M. V. BOUT
Laboratoire d'Astronomie Spatiale, Marseille, France

R. SCHWENN
Max-Planck-Institut für Aeronomie, Lindau, Germany

and

G. M. SIMNETT, D. K. BEDFORD, C. J. EYLES
Space Research Group, School of Physics and Space Research University of Birmingham, Birmingham, U.K.

Abstract. The Large Angle Spectroscopic Coronagraph (LASCO) is a three coronagraph package which has been jointly developed for the Solar and Heliospheric Observatory (SOHO) mission by the Naval Research Laboratory (USA), the Laboratoire d'Astronomie Spatiale (France), the Max-Planck-Institut für Aeronomie (Germany), and the University of Birmingham (UK). LASCO comprises three coronagraphs, C1, C2, and C3, that together image the solar corona from 1.1 to 30 $R_\odot$ (C1: 1.1 - 3 $R_\odot$, C2: 1.5 - 6 $R_\odot$, and C3: 3.7 - 30 $R_\odot$). The C1 coronagraph is a newly developed mirror version of the classic internally-occulted Lyot coronagraph, while the C2 and C3 coronagraphs are externally occulted instruments. High-resolution imaging spectroscopy of the corona from 1.1 to 3 $R_\odot$ can be performed with the Fabry-Perot interferometer in C1. High-volume memories and a high-speed microprocessor enable extensive on-board image processing. Image compression by a factor of about 10 will result in the transmission of 10 full images per hour.

Key words: Sun – Corona – Coronagraph

1. Introduction

The invention of the coronagraph by Lyot (1930) opened the way for observations of the corona at times other than during total solar eclipses. In 1963, R. Tousey flew an externally occulted coronagraph on a sounding rocket (Tousey, 1965). This instrument, with an extremely low stray-light level, enabled observations much farther out into the corona than ground-based Lyot coronagraphs could reach. Since then, several externally occulted coronagraphs have been flown on satellites for long-term continuous coronal observations: OSO-7 (1971-72) (Koomen *et al.*, 1975), Skylab (1973-74) (MacQueen *et al.*,

Solar Physics **162**: 357–402, 1995.

1974), P78-1 (1979-1985) (Koomen *et al.*, 1975), and the Solar Maximum Mission (SMM, 1980-1989) (MacQueen *et al.*, 1980). Each of these coronagraphs showed improved spatial resolution, field-of-view, time resolution, and mission duration.

An externally occulted coronagraph, however, has two basic limitations. First, for a given distance from the occulting disk to the first imaging element, the instrument can only provide images of the corona for a finite distance above the Sun's limb (>1.5 $R_\odot$). At the inner edge of the field of view, most of the imaging element is shadowed by the occulter. Consequently, the spatial resolution in the inner corona is poor because of the very small effective apertures. Second, because of size limitations, the aperture cannot usually exceed a few centimeters.

The LASCO coronagraph overcomes these problems by using three different coronagraphs with three overlapping fields-of- view. The inner corona, from 1.1 to 3 $R_\odot$, is imaged by a mirror version of the classic Lyot coronagraph without an external occulter, thus preserving the full resolution of the instrument over the whole field-of-view. The use of reflecting optics in a coronagraph was first suggested by Newkirk and Bohlin (1963) in order to overcome inherent problems with stray light in refractive coronagraphs. The second coronagraph C2 images the Sun from 1.5 to 6 $R_\odot$. The rapidly decreasing coronal intensity with distance necessitates its design as an externally occulted instrument. LASCO extends the field-of-view to 30 $R_\odot$ from the previous maximum of 10 $R_\odot$ by adding a third coronagraph C3. The C2 coronagraph overlaps the outer field-of-view of the C1 coronagraph and the inner field of view of C3 in order to maintain the ability to obtain high spatial resolution images over the whole field from 1.1 to 30 $R_\odot$.

LASCO will be the first spaceborne coronagraph with spectroscopic capabilities. C1 is equipped with a Fabry-Perot interferometer that can take monochromatic images over the entire field-of-view with a spectral resolution of 0.07 nm. By stepping the bandpass across a spectral line, line profiles and Doppler shifts can be derived for all 1024×1024 pixels simultaneously.

2. Optical Design of the Three Coronagraphs

2.1. The C1 coronagraph

Lyot (1930) identified five sources of scattered light in an ordinary objective lens telescope:

1. diffraction at the aperture of the lens,
2. a spurious solar image produced by multiple reflections in the objective lens,
3. macroscopic inhomogeneities in the glass,
4. surface inhomogeneities of the lens (pits, scratches), and
5. body-scattering within the glass.

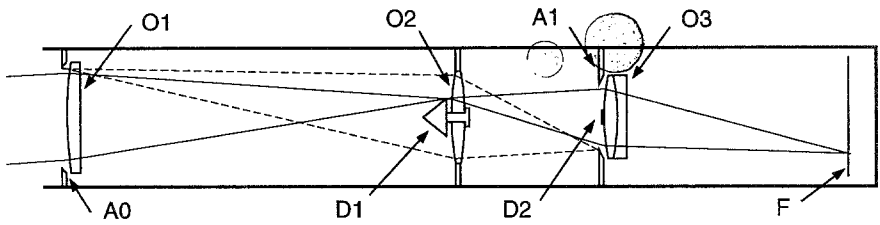

Fig. 1. Optical components of the Lyot coronagraph: entrance aperture A0; objective lens O1; internal occulter D1; field lens O2; Lyot stop A1; Lyot spot D2; objective lens O3; and focal plane F.

This analysis led Lyot to invent the coronagraph. Figure 1, following Evans (1953), illustrates the design principle which aims to reduce the scattered light resulting from items 1 and 2 above. A solar image is formed by the objective lens O1 at the internal occulter D1, where the photospheric light is blocked by a highly reflecting metal cone. A field lens O2 images the entrance aperture O1 and its diffraction pattern onto the Lyot stop A1, which prevents most of the diffracted light from reaching the focal plane. The inner occulter D2 (the Lyot spot) blocks the spurious solar image caused by multiple reflections in the objective lens. With this design, Lyot found that he could eliminate stray light caused by aperture diffraction and by multiple reflections in the objective lens, which are the major contributors to the scattered light in a telescope with a clean, well-polished lens. The other three stray-light sources mentioned above remain but could be reduced by selecting very clear glass and polishing it well. Lyot constructed coronagraphs with a residual scattered light level of 5×10^{-6} $B_{\odot}$. Since the level of scattered skylight on a very high mountain top is seldom less than 10×10^{-6} $B_{\odot}$at visible wavelengths, coronal observations with ground-based Lyot coronagraphs are sky background limited rather than instrument background limited.

Coronal observations from space are limited only by the scattered light generated within the instrument. So far, all space-based coronagraphs have been externally occulted instruments that use a principle first described by Evans (1948). Because of dimensional constraints of current spacecraft, it is not possible to build a sufficiently long externally occulted coronagraph to observe the innermost corona with high spatial resolution. With the advent of superpolished mirrors and extremely smooth coatings, a new modification of the Lyot coronagraph is possible (here called the mirror Lyot coronagraph). Figure 2 shows the optical layout of the LASCO C1 coronagraph. An off-axis, superpolished, parabolic mirror M1 forms an image of the Sun on a convex mirror M2. All of the photospheric light passes through a hole in M2 and is subsequently dumped outside the instrument. A1 is both the Lyot stop and the aperture stop. A0 and the diffraction pattern from its edge are imaged by M1, M2, and M3 (another off-axis parabolic mirror) at

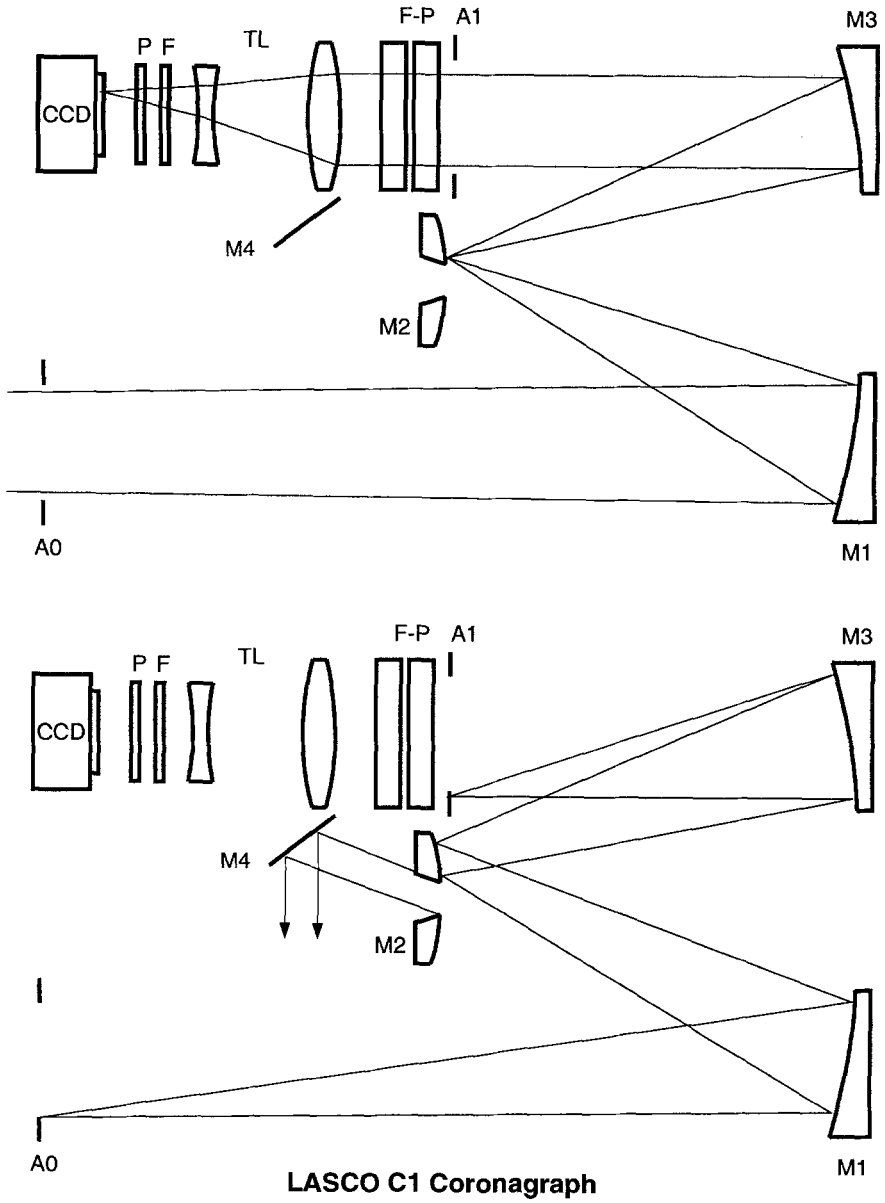

Fig. 2. Mirror Lyot coronagraph: Top, coronal imaging; entrance aperture A0; off-axis parabolic mirror M1; first image plane and convex mirror M2; off-axis parabolic mirror M3; disk light rejection mirror M4; Lyot stop A1; Fabry-Perot interferometer F-P; telephoto lens TL; blocking filters F; polarizers P; CCD detector. Bottom, suppression of stray light. Diffracted sunlight from the edge of A0 is imaged on the Lyot stop A1. The solar image is discarded via a hole in the field mirror M2

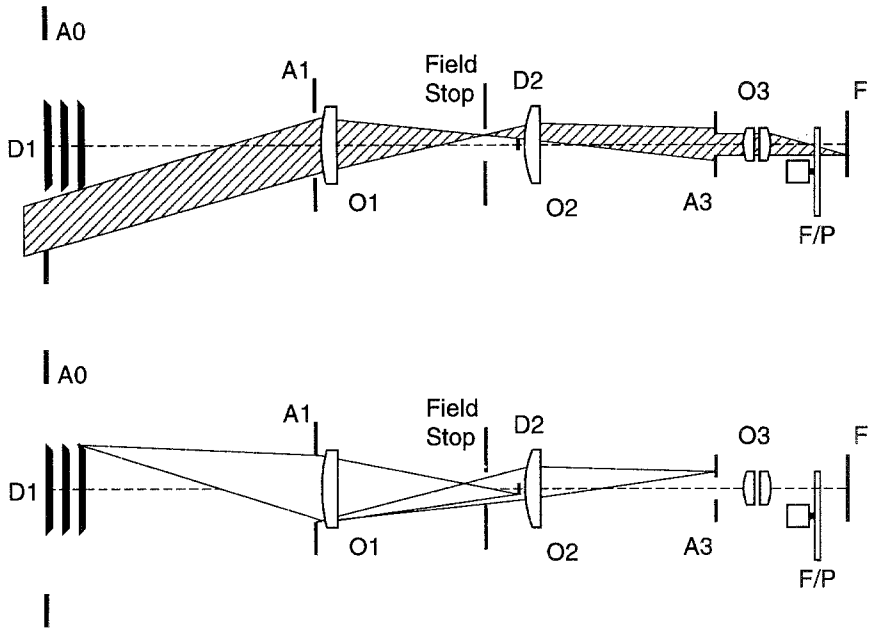

Fig. 3. Externally occulted Lyot coronagraph: front aperture A0, external occulter D1, entrance aperture A1, objective lens O1, internal occulter D2, field lens O2, Lyot stop A3, relay lens with Lyot spot O3, filter/polarizer wheels F/P, and focal plane F.

A1, where the Lyot stop blocks the light diffracted from A0. The mirror M1 has been sized larger than the solar beam, and, consequently, the aperture A0 is the only source of diffracted light. Since there are no multiple reflections in the mirror Lyot coronagraph, the inner Lyot spot can be omitted. A Fabry-Perot interferometer F-P is located in the parallel beam behind the Lyot stop at A1. The telephoto lens TL images the corona onto the CCD detector. Blocking filters for the interferometer are inserted into the beam at F, and polarizers are inserted at P.

2.2. The C2 and C3 coronagraphs

A conceptual diagram for C2 and C3 is illustrated in Figure 3. The top diagram traces a selected ray bundle for the coronal image, while the bottom diagram illustrates the optical elements and ray paths involved in the suppression of stray light. Beginning at the left of each diagram, the external occulter D1 completely shadows the entrance aperture A1 from direct sunlight. For the C3 coronagraph D1 consists of three circular disks on a common spindle, the disks being sized and spaced so that each intercepts the diffracted sunlight from the edge of the one before, to minimize the total of diffracted light falling on A1. For the C2 coronagraph, D1 is a tapered cylinder with a finely polished screw thread to imitate multiple disks.

TABLE I
System Parameters for C1,C2,C3

	Field of View ($R_\odot$)	Occulter Type	Spectral Bandpass	Objective Element	Pixel Size	Brightness Range $B_\odot$
C1	1.1 - 3.0	Internal	Fabry-Perot	Mirror	5.6"	2×10^{-5} to 2×10^{-8}
C2	1.5 - 6.0	External	Broadband	Lens	11.4"	2×10^{-7} to 5×10^{-10}
C3	3.7 - 30	External	Broadband	Lens	56.0"	3×10^{-9} to 1×10^{-11}

The objective lens O1 images the corona the field stop which defines the outer field limit (6.0 $R_\odot$ for C2 and 32 $R_\odot$ for C3). The O1 objective lens also images D1 onto a stop D2 at a distance behind the coronal image. This D2 internal occulter intercepts residual diffracted light originating at the edges of D1. A short distance behind D2 is a field lens O2, which collimates the primary coronal image, and also images A1 onto the Lyot stop A3. The Lyot stop intercepts diffracted light originating at the entrance aperture A1. Finally, a relay lens O3 behind A3 re-images the primary coronal image onto the 1024x1024 pixel CCD camera at the image plane F. The front surface of the O3 relay lens also carries the Lyot spot. The Lyot spot for the externally occulted coronagraphs intercepts residual diffracted light from D1, imaged on the spot by inter-reflections in the O1 objective lens. Color filters and linear polarizing filters (F/P) are carried on two wheels in front of the focal plane.

Table 1 summarizes the design parameters of the three coronagraphs.

2.3. Stray Light in C1, C2 and C3

Stray light levels for all three instruments have been measured in a special vacuum facility at the Naval Research Laboratory (NRL). The laboratory values are shown in Figure 4 where they are compared with expected coronal signals. It has been demonstrated that the stray light level of C1 is solely determined by the surface quality of the first mirror M1. At 3 $R_\odot$ the stray light level of 10^{-8} should be low enough to produce eclipse-like images. The signal to stray light level of 1:1 in C1 should produce images with very high contrast values. C2 and C3 have stray light levels which are an improvement of at least an order of magnitude over previously flown coronagraphs. As Figure 4 shows, the C2 and C3 stray light levels at all distances from the Sun are at least an order of magnitude below the anticipated coronal signal.

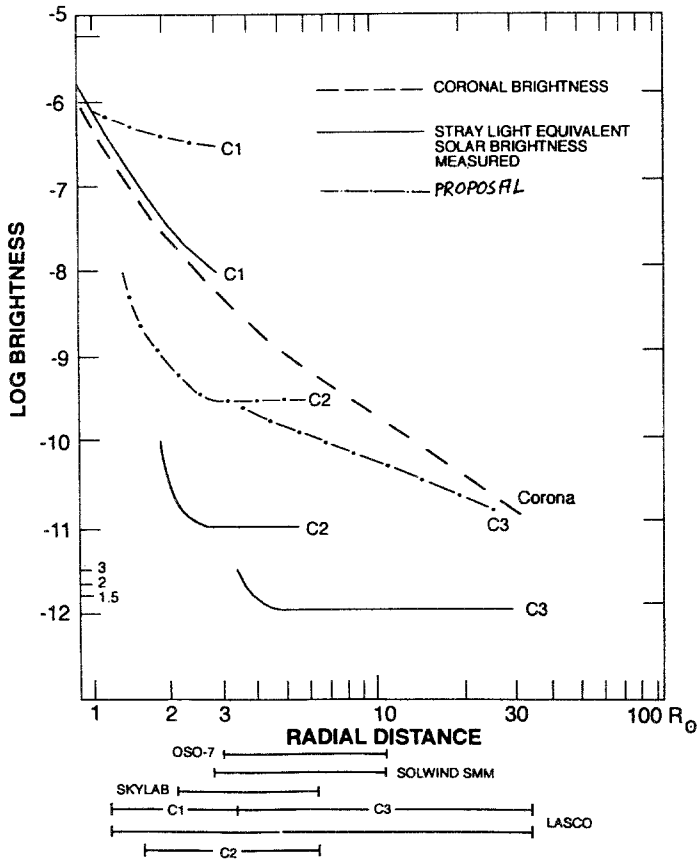

Fig. 4. Measured Stray light levels in C1, C2 and C3 *vs.* the K+F corona. The fields of view of previous coronagraphs are indicated.

They are also considerably below the levels that were considered possible in the original LASCO proposal to NASA.

2.4. Spatial resolution of the coronagraphs

As mentioned above, the internally occulted coronagraph was designed to obtain coronal images with full instrumental spatial resolution over the entire field-of-view which extends as close to the solar limb as possible. The spatial resolution of C1 is determined primarily by the detector pixel size with respect to the plate scale. The equivalent pixel size of the CCD is 5.6 arc-sec. and the spatial resolution is then approximately 11 arc-sec. The limiting aperture is the Lyot stop A1 and the Rayleigh diffraction limited resolution is 3.3 arc-sec. at 530.3 nm.

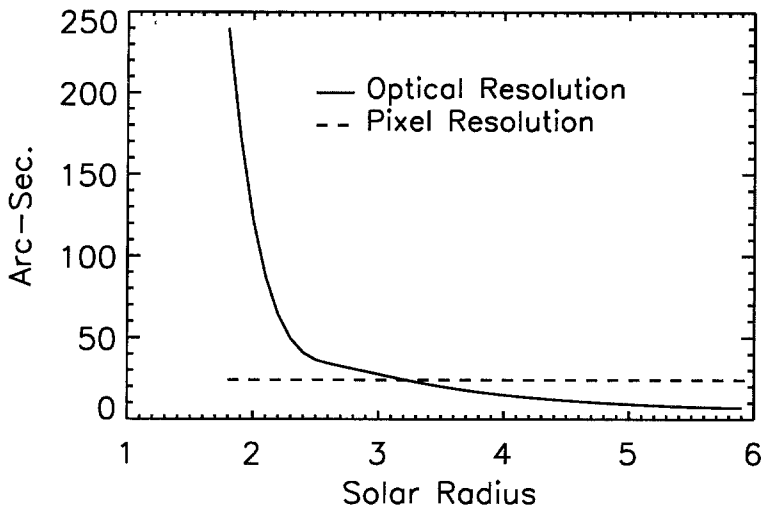

Fig. 5. Optical and pixel resolution of C2. (Pixel resolution is equivalent to the size of two pixels.)

Figures 5 and 6 show the calculated optical resolution of C2 and C3, respectively. Vignetting at the inner edge of the field-of-view is responsible for the loss in spatial resolution in the inner field.

3. Detailed Design of C1

The optical layout of C1 is shown in Figure 7. The entrance aperture A0 (4.7 cm diameter) allows the full Sun and the corona to illuminate the off-axis parabolic objective mirror M1 (75 cm focal length). A real image of both the Sun and the corona is formed at mirror M2 which acts as a field mirror. The photospheric light is allowed to pass through a hole (equivalent radius 1.1 $R_\odot$) in M2. This light is eliminated from the telescope with the diagonal rejection mirror M4 and a subsequent optical relay. The coronal light is reflected from M2 on to the off-axis parabolic mirror M3. The two parabolic mirrors, M1 and M3, which are placed symmetrically, form segments of a single parabolic mirror and serve to eliminate coma. The field mirror M2 is spherical (242.2 cm radius of curvature). The combination of M1, M2 and M3 produces a real 1:1 image of A0 at the stop A1. The M1 aperture is sufficiently larger than A0 that light originating at the edge of A0 is intercepted. In this way, A1 functions as a Lyot stop. The collimated beam leaving A1 is sent through a narrow-bandpass tunable Fabry-Perot interferometer FP described later.

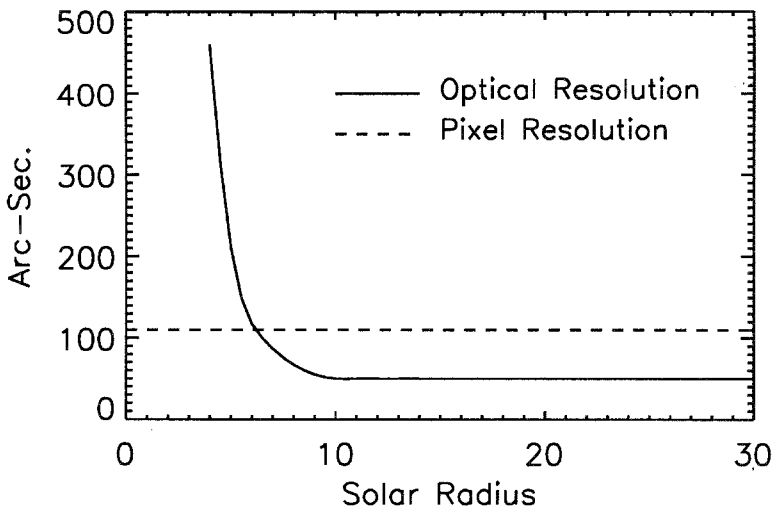

Fig. 6. Optical and pixel resolution of C3. (Pixel resolution is equivalent to the size of two pixels.)

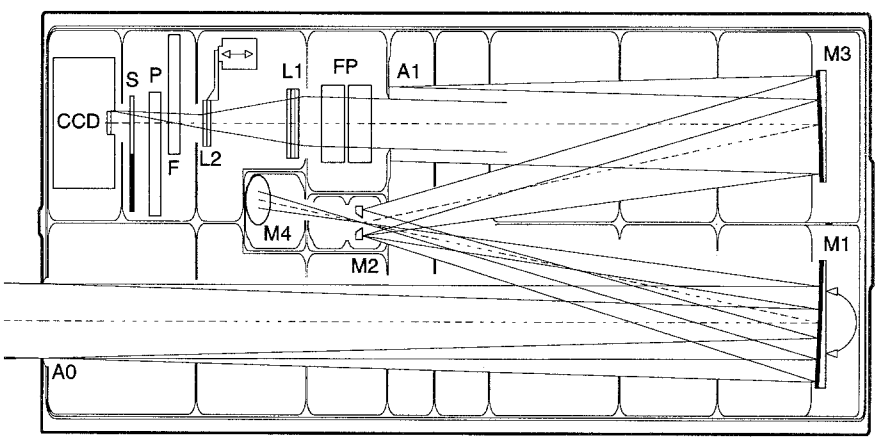

Fig. 7. The C1 coronagraph (not to scale)

The C1 Lyot mirror coronagraph telescope design has a number of attractive features. With the selection of a mirror objective instead of a lens, the difficulties with multiple internal reflections, bulk scatter, browning and fluorescence are entirely avoided. Additionally, the singlet objectives typically used in most coronagraphs require considerable overoccultation because of chromatic aberration present at the solar disk. This chromatic aberration must then be corrected later in the focal plane package to obtain coronal

images of acceptable quality. In contrast, the M1 mirror forms a high quality, achromatic, image of the solar disk which is then cleanly eliminated with the M2 field mirror. The comatic aberration present at M2 is canceled by its reflection at M3. The naturally folded design is compact and was easily accommodated within a small envelope. Instrument pointing errors are readily corrected without inducing substantial aberrations by tilting the M1 mirror. Dynamic imaging is possible with the same technique. These design considerations and the promise of excellent quality, low scatter aspheric mirrors led to the selection of a reflective design over the more classical lens design for the C1 telescope.

A telephoto lens system (76.8 cm focal length) consisting of 5 lenses in 2 groups (L1 and L2 in Fig. 7) forms the actual coronal image. The backside group of the telephoto lens can be moved along the optical axis by a motor-driven mechanism, should refocusing be required. The coronal light passes through a system of broad-band filters and polarizers mounted on two filter wheels. The final image is formed on a CCD camera located behind a mechanical shutterblade. The layout is such that a circular field of view with a radius of 3 $R_\odot$ forms an inscribed circle on the 1024×1024 pixel CCD where one pixel subtends 5.6 arc-sec. in the corona.

The optical design of the C1 coronagraph was optimized by evaluation of spot diagrams from geometrical ray tracing calculations. The limiting spatial resolution for a single exposure is about 11 arc-sec. (2×5.6 arc-sec. pixels) and is determined by the pixel size. For multiple exposures of the same scene, the CCD limited resolution performance can be increased by about a factor of 2 by using dynamic imaging. In this mode the M1 mirror is tilted between exposures such that the corona in the image plane is shifted by half a pixel in both the x and y direction. After a total of 4 exposures, the effective resolution is nearly doubled. This has been confirmed in optical tests of the integrated telescope.

Optimum suppression of stray disk radiation requires clean removal of the disk radiation with one reflection. Selection of a parabolic mirror for M1 instead of a sphere allows removal of the solar radiation while still permitting observation of the innermost corona. The spot size on M2 of any point on the solar limb is about 0.070 mm and is equivalent to 20 arc-sec. or 0.02 $R_\odot$. In order to maintain a safe margin between the limb and the coronal field of view, the equivalent radius of the occulting hole in M2 is 1.1 $R_\odot$.

The front apertures of the three instruments are each covered by motor-driven dust-tight doors. The C1 door lid contains a quartz diffuser. When the door is closed, attenuated, diffuse light from the solar disk illuminates A0 and is transmitted through the telescope to the focal plane. This radiation provides flat field images with solar spectral content for instrument in-flight calibration. The spectra obtained with the door closed provide solar refer-

ence spectra for later use in removal of mean stray radiation background from the coronal emission line images.

The main mirrors M1 and M3 are off-axis parabolic mirrors made of Zerodur. The optical surfaces were polished to a micro-roughness of 0.2 nm r.m.s. With considerable effort several mirrors were produced by two manufacturers - Zeiss (Oberkochen, Germany) and REOSC (Ballainvilliers, France) - with ever increasing surface quality. The mirror selected for use as M1 (made by Zeiss) had a measured r.m.s. micro-roughness of 0.084 nm before coating and 0.104 nm r.m.s. afterward. The less critical M3 mirror is from REOSC. The mirror coatings (100 nm Al with a 200 nm SiO_2 protective layer) were performed by General Optics Inc., Moorpark, USA.

The reflectivity of the Al coating is about 92% so that 0.190 W of the incident 2.38 W incident power is absorbed by M1. Active cooling of M1 was considered unnecessary and M1 will be operated under somewhat enhanced equilibrium temperatures in order to help reduce the risk of molecular contamination. M1 is mounted in a piezo-electric driven mechanism which allows M1 to be tilted in all directions in steps of 1.4 arc-sec. through an angle as large as 1 arc-min. This allows C1 to perform pointing corrections and dynamical imaging.

The field mirror M2 is made from stainless steel with a 40 nm Al coating protected by a 10 nm SiO_2 coating. The center hole (front diameter 7.68 mm) is conical, with a knife edge in front. This edge shows up brightly in the inner portion of the CCD and is superposed on the bright image of the inner corona. In order to avoid overexposure a radial neutral density filter is employed on M2. That was achieved by a gradual thinning of the coating towards the edge. Inside 1.3 $R_\odot$, the reflected intensity smoothly drops to about 10% of the value at the 3 $R_\odot$ edge.

Two filter wheels and the shutter mechanisms are contained in a combined unit called the 'triple mechanism'. Each of the two filter wheels holds five filters and these are listed in Table II. The color filter wheel F holds the four Fabry-Perot blocking filters plus an orange wide band filter. The polarizer wheel P contains three linear polarizers with axes oriented 60° apart. The fourth position holds an Hα filter which works in conjunction with the orange filter on the other wheel. The fifth position holds a clear glass which, in conjunction with the orange filter, provides for visible light images of the corona. The mechanical shutter S is of the 'windmill type'. In its closed position, the shutter keeps the CCD dark in order to obtain dark image exposures both on the ground and in orbit.

3.1. C1 Test and Calibration Results

During the development phase the new optical design was tested, improved, and verified in several iterative steps. The basic debugging and optimization work was done using a prototype telescope that was later on turned into a

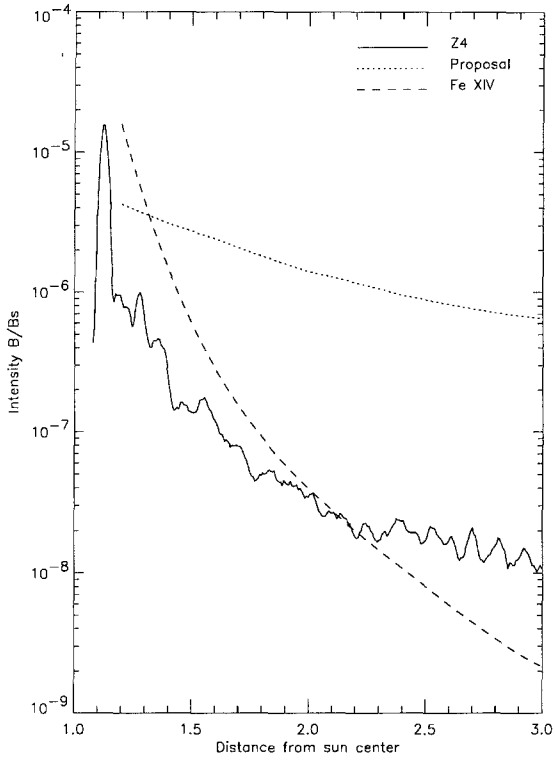

Fig. 8. Stray light measurements for the C1 coronagraph

working telescope and used at Pic du Midi, Sacramento Peak and Mauna Loa. This work included the development of appropriate integration, calibration, and test procedures under the conditions of a class 100 cleanroom.

A dedicated solar simulation facility was set up for performing straylight measurements of the main mirrors in order to allow selection of the best units for flight. A further solar simulation device included both an extended 'Sun' source and a narrow laser beam. It was permanently installed in the integration cleanroom, for repeated checkout of alignment and optimum straylight performance during all steps of integration work. As shown in Figure 8, the straylight level stays below the average coronal Fe XIV brightness (solid curve) out to 1.8 $R_\odot$, and at 3 $R_\odot$ it is as low as 10^{-8} solar $B_\odot$.

Before the actual flight model was finally integrated an exact true to scale unit (the 'lab model') was assembled and carefully tested, using all the optical flight elements or their spare units (except for the Fabry-Perot interferometer and the CCD camera which were inserted later directly into the flight model). After all these preparations, the assembly and testing of the flight model in Lindau was fairly straightforward.

TABLE II
C1 Filter Wheel and Polarizer Wheel

Hole	FILTER WHEEL	POLARIZER WHEEL
1	Na I	-60°
2	Fe XIV	0°
3	Ca XV	+60°
4	Fe X	clear
5	Orange	Hα

The telescope was then shipped to and completed in the NRL facilities. There the final integrations and adjustments, optical tests, and calibrations with the instrument in final configuration were performed: 1. alignment of the C1 optical axis with the C1 boresighter, 2. coalignment with the C2/C3 optical axis (by adjusting the M1 ground position), 3. straylight test with an artificial (white) Sun in the vacuum tank and a cooled CCD, 4. flat field calibration with an external photometrically calibrated flat field in all relevant filter permutations, 5. flat field calibration with the in-flight source, i.e. diffuser window in front door, for reference with 4, 6. flat field calibration with additional light sources built in the telescope to illuminate the diffuser window internally, 7. focusing tests in air and in vacuum, and 8. dynamic imaging.

The overall straylight distributions are symmetric around the occulting hole and do not show any disturbing peculiarities. The absolute levels are low. The flat field images are actually flat, i.e. there are no hot pixels due to faults in the filters or the CCD nor are there significant interference patterns. Refocusing in orbit, if necessary, will be relatively straightforward since the occulter edge serves as an ideal focusing target.

By obtaining a sequence of images at slightly offset pointing, it is possible to build up a combined image having resolution superior to that of a single image. The M1 mirror mechanism is used to tilt the mirror so that a reference image, an image offset 1/2 pixel in the horizontal direction, an image offset 1/2 pixel in the vertical direction, and an image offset 1/2 pixel in both directions are obtained. The four images are combined to produce a high resolution image. This technique has been demonstrated during ground testing of C1 as shown in Figure 9. Here, images of a fine wire mesh were obtained. On the left, the image derived from a single exposure is shown, at normal resolution at the top. The image at the bottom is highly magnified to highlight the individual pixels. On the right is shown an image derived from four offset exposures. The superior resolution of the mesh grid is quite evident.

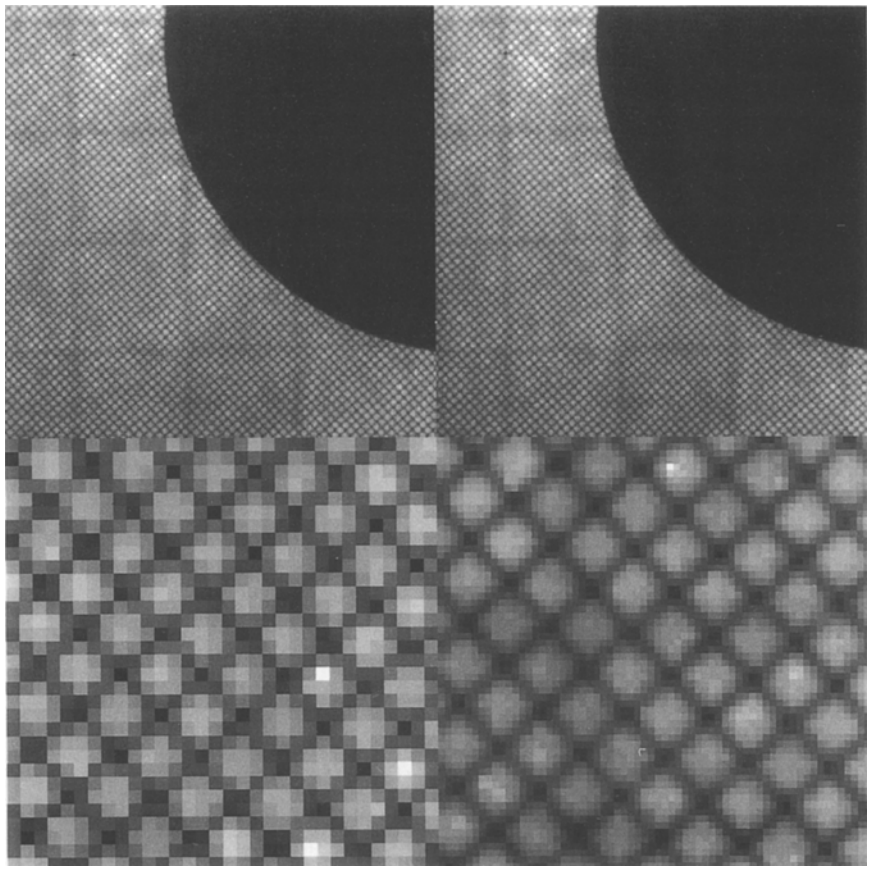

Fig. 9. C1 test images of a fine wire mesh. On the left, images from a single exposure and on the right, images from a 'dynamical imaging' sequence of four exposures.

4. The C1 Fabry-Perot Interferometer

The C1 tunable filter system allows narrow passband images of the solar corona to be obtained simultaneously over the entire 1.1-3.0 $R_\odot$ field of view. The system consists of a piezo-electrically scanned Fabry-Perot interferometer used in combination with a set of blocking filters. Each blocking filter selects a specific emission line spectral neighborhood and blocks all but a single transmitted interferometer order. The divergence of the collimated beam in C1 allows the full-width half-maximum of a single, annular interferometer Haidinger fringe to span the annular (1.1 - $3R_\odot$) telescope field of view. The central wavelength of the fringe is selected for each exposure by tuning the interferometer cavity length to a specific stationary value. The

blocking filters minimize the out-of-band continuum and were measured to have $>10^5$ out-of-band rejection. The out-of-band performance of these filters is particularly significant because the CCD detector is sensitive from 400 to 1100nm.

The tunable Fabry-Perot interferometer and the C1 telescope system are well matched for the observational objective of obtaining narrow bandpass images over a wide field of view. The tunable Fabry-Perot design was selected over a dispersive spectrograph design because it allows C1 to operate as a relatively high luminosity spectrometer (Jacquinot 1954). The location of the interferometer near the telescope aperture stop A1 minimizes the impact of local variations in the interferometer transmittance profile over the Fabry-Perot aperture. All interferometer cavity spatial defects are summed into a single interferometer profile which is uniformly distributed over the field of view. The high luminosity of the combined telescope and filter system design allows reasonable photon count rates to be achieved over the entire field of view. The instrument develops an acceptably high signal-to-noise ratio within sufficiently short exposure times to allow detailed observation of the evolution of coronal structures.

The Fabry-Perot interferometer cavity length and parallelism directly affect the filter passband central wavelength and shape, respectively. Significant cavity length drift results in variations of the effective passband central wavelength. Lack of parallelism reduces the instrument finesse and consequently broadens the transmission profile. In order to control these cavity parameters, the Fabry-Perot interferometer cavity length and parallelism are monitored with capacitance micrometers and adjusted with piezo-electric transducers (PZT). This control system forms the fast inner stage of a nested two stage closed loop control system. The capacitance micrometer pads were deposited directly on the interferometer substrates for stability and compactness. Small drifts in the capacitance micrometer electronics result in the interferometer plates gradually moving from their ideal positions.

Consequently, the interferometer is also optically monitored with a second stage to correct for electronic drift at regular intervals. The performance of the interferometer is gauged by analyzing the shapes of observed solar spectral features, typically Fraunhofer lines. These data, used for feedback in the outer stage, are acquired with two separate optical systems. The first optical system is the C1 instrument itself whose coronal images, formed at the CCD, contain the background Fraunhofer spectrum scattered by the primary mirror (M1). This optical system is the primary feedback for the tunable passband control system. The spectral information is used for interferometer finesse optimization and an absolute wavelength standard for Doppler velocity measurements.

Although used as the fundamental performance baseline, continuous monitoring of the interferometer performance with the CCD at regular interval

is not practical. To preserve the great majority of LASCO's operations for scientific observations, a second, fast feedback optical system, called the optical control channel (OCC) system is employed. The OCC system monitors the disk Fraunhofer spectrum contained in the diffracted light originating from the edges of three slots in the telescope entrance aperture panel. The edges of the three slots are imaged on three small apertures at the Lyot stop. This light is passed by the interferometer at three points around the cavity perimeter and sampled by three photodiodes mounted on the interferometer structure. Each optical control channel contains a blocking filter to isolate a single interferometer order in the neighborhood of the 543.5 nm absorption line. The OCC system maintains the interferometer electronic adjustments determined from CCD scans. The OCC system is used to monitor the cavity condition during each coronal science image readout from the CCD. Using the 543.5 nm absorption line, it provides a secondary feedback which corrects for electronic drift with a repetition period much less than the interferometer electronic stability time constant. The secondary OCC system feedback will deviate from the primary instrument system feedback only when the optical properties of the C1 instrument change.

The basic C1 observing mode will be to step the Fabry-Perot interferometer through a sequence of wavelengths that span the selected line profile and its nearby continuum. One or more camera exposures are read out at each step. The number and size of the wavelength steps will be chosen to optimize a particular observing sequence. The minimum filter central wavelength step is about 0.0035 nm. Removal of the stray disk radiation from the E- and K-coronal images requires knowledge of the shape of the photospheric spectrum which characterizes the background radiation scattered by M1 and any contribution from the F-corona.

For the coronal emission lines, it will also be necessary to know the shape of the photospheric spectrum which forms a large component of the underlying background radiation. The shape of this spectrum will be measured from the light passed by the diffuser when the instrument door is closed. The polarization properties of the coronal radiation will be measured by inserting linear polarizers (0, $\pm 60°$) into the beam.

A central objective of the LASCO instrument is to obtain the first high quality synoptic measurements of coronal line profiles and intensities over a wide field of view. The line profile measurements will be used to obtain bulk flow and turbulent velocities of structures in the inner corona. Relatively large ($\sim$100 km s^{-1}) velocities have been previously measured during transient events in the corona. The requirement to observe these large velocities determines the tunable range of the filter system. The tunable range must also be large enough to include the Doppler shifts expected from the solar wind expansion velocities as well as for coronal mass ejections. A similar tunable range is required for the photometric K-corona measurement method

TABLE III
Wavelength bands of C1

Fabry-Perot Interferometer				
Channel	Wavelength	Spectral Resolution	Tunable Range nm	km s^{-1}
Fe XIV	530.3 nm	0.065 nm	±0.76	±430
Ca XV	564.9 nm	0.059 nm	±0.92	±485
Na I	589.0 nm	0.072 nm	±0.81	na
Fe X	637.4 nm	0.085 nm	±1.06	±500
Hα	656.2 nm	0.104 nm	±1.12	±512
White Light	530-640 nm	0.065 nm	na	na

developed by Grotrian (1934). The interferometer passband FWHM was matched to the expected line widths in order to operate with maximum efficiency. The passband FWHM (spectral resolution) and tunable range of the interferometer are given in Table III for the various blocking filters. Models of coronal intensities have been used to estimate the expected precision of the doppler measurements as shown in Table IV.

Another important goal of the LASCO observations will be to determine the degree and direction of polarization of the coronal emission lines and white light corona. For example, polarization analysis may be used as an independent method to separate the K corona from the F corona and stray radiation. The results from the Grotrian method are further enhanced if the polarization is determined. The direction of the coronal magnetic field may be inferred from the polarization in the Fe XIV 530.3 nm line.

5. Detailed Design of C2

A primary goal of C2 is to detect the corona as close as 2 $R_\odot$ from Sun center. In order to do this, considerable attention has been given to the suppression of stray light in the instrument. This is achieved, to a large extent, by the proper optimization of the external occulter, the objective lens O1 and its aperture, and the internal occulter.

A new type of external occulter has been introduced in C2 consisting of multiple (160) sharp threads diamond-machined on a cone whose angle slightly exceeds that subtended by the Sun at the L1 Lagrangian point (32.31 arc min, average value). Extensive laboratory tests have shown that this occulter achieves a rejection of 1.5×10^{-5} (Lamy et al., 1994). At this level, the light diffracted by the entrance aperture A0 becomes a major

TABLE IV
Expected precision of emission line measurements

	Fe X λ637.4		Fe XIV λ530.3		
$r/R_\odot$	Intensity	Velocity	Intensity	Velocity	Exposure
1.1	0.9%	0.05 km s^{-1}	3%	0.1 km s^{-1}	60 s
1.5	1.2%	0.13 km s^{-1}	3%	0.6 km s^{-1}	60 s
2.0	5%	1.0 km s^{-1}	6%	1.4 km s^{-1}	60 s
2.5	24%	1.8 km s^{-1}	15%	2.1 km s^{-1}	60 s
3.0	48%	8. km s^{-1}	28%	2.7 km s^{-1}	60 s

concern. This has been solved by introducing a serrated design: each side of the polygon behaves as a short knife-edge whose direct diffraction avoids O1. Although the remaining light scattered by minute imperfections of the knife-edges is very low, the total contribution as observed in the conjugate plane exceeds that of the external occulter. An oversized internal diaphragm A2 prevents further propagation of this stray-light.

The two-element design (doublet) introduced on SMM (MacQueen et al., 1980) reduces chromatism and therefore allows more efficient inner occultation. In addition, several innovative solutions have been implemented to limit the light scattered by the objective itself. First, all surfaces have been superpolished such that the r.m.s. value of the remaining roughness amounts to a few 0.1 nm. Second, the two elements are in optical contact to minimize multiple reflections between the internal faces which were a major problem in the SMM air-spaced design. Third, the external faces have been anti-reflection coated using ion-assisted deposition. Laboratory measurements have shown that this proprietary technique developed by PMS (Boulder, CO) does not introduce any degradation of the quality of the optical surfaces. The integrated light scattered by the O1 objective as measured at the A1 aperture (and which effectively propagates in the instrument) amounts to 5×10^{-5} of the illuminating source. In the conjugate plane of the external occulter, the image of the bright fringe which surrounds it is apodized by an inner occulter D2. The over-occultation of 10% results from a compromise between straylight rejection which controls the detection of the corona in the outer part of the field-of-view and the vignetting which determines the spatial resolution in the inner part.

The field objective O2 is a standard two element design and images the O1 plane in order to perform two functions. First, the light diffracted by the O1 aperture A1 is apodized by a final diaphragm oversized by 4%. Second, the ghost images created by the O1 objective are blocked by a Lyot spot. Optical

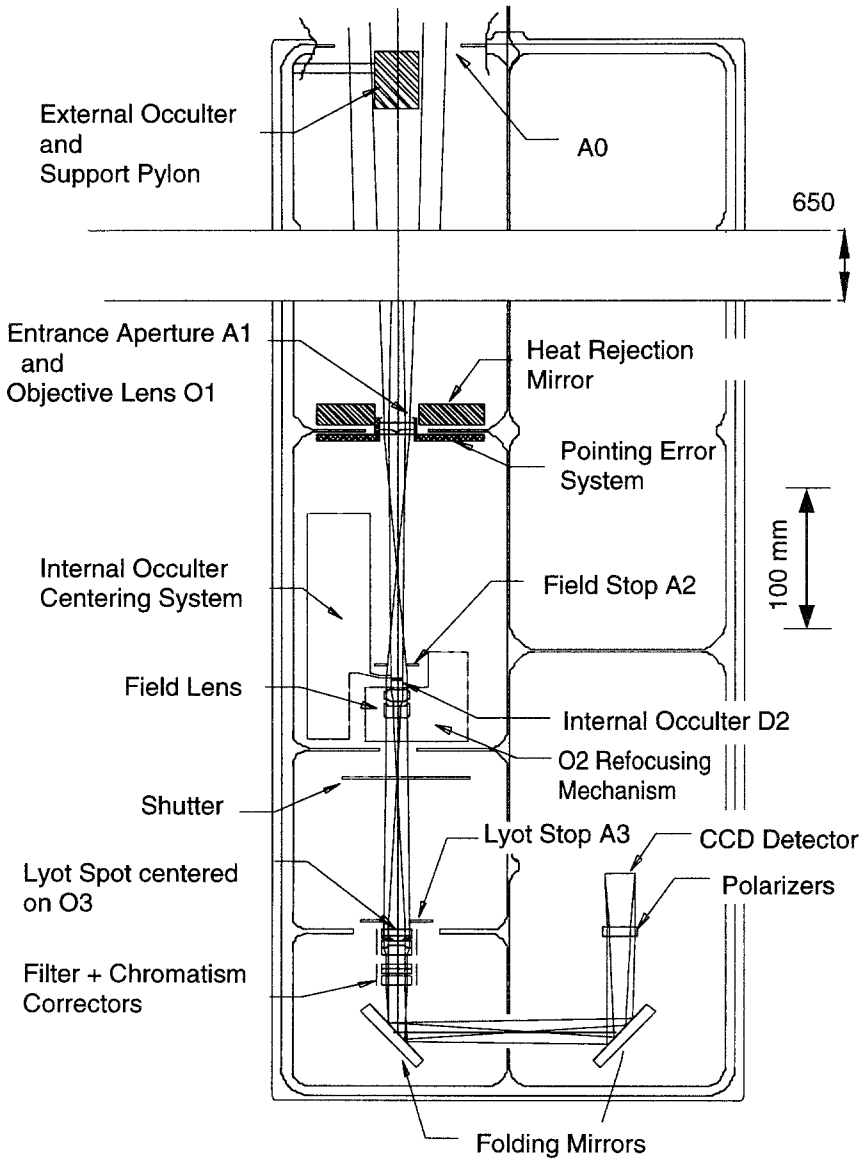

Fig. 10. The optical layout of the C2 coronagraph

calculations confirmed by laboratory measurements have shown that these ghosts amount to approximately 2×10^{-10}. They are blocked by a circular metallic layer deposited on the front surface of the final relay or imaging objective O3. The relay consists of a four-element design which relays and magnifies the primary image of the corona seen through O2 onto the CCD detector. Two plane mirrors M1 and M2 fold the optical path in order to limit the overall length of the instrument. They have received a special anti-

reflection coating to reduce their polarization to a few percent. The shutter and the filter wheel are mounted as close as possible to the final pupil, the former in front and the latter just behind the O3 objective, while the polarizer wheel is placed near the image plane, in front of the CCD camera.

Although not directly part of the coronagraph design, two additional optical components play a critical role in the overall performances of the system. First, the heat rejection mirror, which collects all direct sunlight entering the instrument, focuses the solar image in between the external occulter and the A0 aperture and rejects it outside. It is a slightly tipped spherical, first surface mirror made of super-polished kanigened aluminum (a substrate of aluminum with a 0.05 mm nickel overcoat) and protected by a proprietary coating (alflex-a) made by Balzers (Liechtenstein). This design minimizes the light scattered into the light tube and onto the rear of the external occulter, which would in turn illuminate the O1 objective. Second, the light tube itself does not operate as a baffle since the internal vanes lie in the shadow of the entrance aperture. Its design prevents diffuse or reflected light resulting from simple or double reflections on the tube from falling inside the A1 aperture.

The detection of the corona in the inner part of the field-of-view depends critically upon the balanced apodization of the bright fringe of the external occulter. A centering mechanism allows the inner occulter to be moved in two orthogonal directions with a step size of 4 microns. Total displacement of 400 microns in the four directions allow four arcs of the fringe of the external occulter to be successively uncovered. These can be imaged onto the detector by means of a special lens in the filter wheel and a neutral density filter in the polarizer wheel. This will be occasionally used to adjust the pointing of LASCO to the Sun should an anomaly be detected. The routine control of the pointing will be achieved by the 'pointing error system', an opto-electronic, fully redundant system which will detect any imbalance in the penumbra created by the external occulter around O1 and generate an error signal. The light going through four holes symmetrically located around O1 falls onto four photodiodes; the differential output of two diametrically opposed diodes is amplified, coded and telemetered to the ground for analysis as the system works in open-loop. Ground commands to move the pointing legs will be sent until a satisfactory pointing is achieved.

In-flight calibrations will be achieved in several ways. First, a combination of an opal and a neutral density filter inserted in the aperture door will provide diffuse, attenuated solar light equal to 6×10^{-10} $B_{\odot}$. Second, stars down to the 8th magnitude and planets (especially Mercury) will be observed as they transit the field-of-view. Numerical simulations have shown that, in spite of the degraded image quality imposed by the occulter, an excellent photometric accuracy may be obtained on stellar and (quasi stellar) planetary images (Fang et al. 1994). Finally, a working calibration is provided by

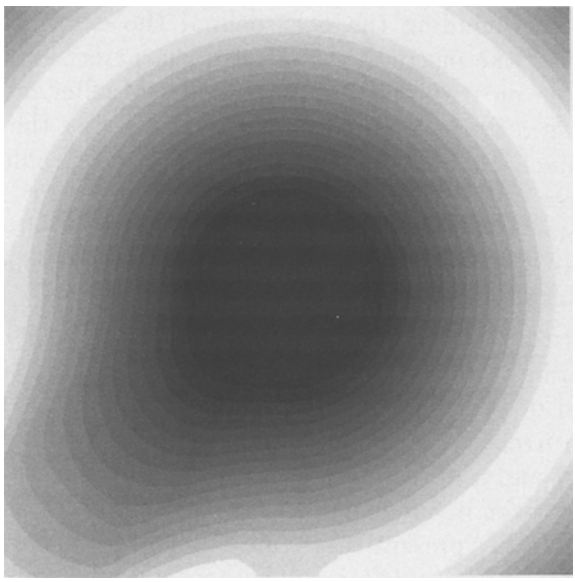

Fig. 11. The two-dimensional vignetting function of C2.

a redundant set of two diametrically opposed lamps illuminating the back face of the shutter blade which acts as a diffuser.

6. Test Results of C2

The C2 coronagraph has been extensively tested and calibrated first at the Laboratoire d'Astronomie Spatiale and second at NRL where vacuum facilities are available. It is beyond the scope of the present article to report the detailed results of the calibrations which have involved the processing of thousands of images. We limit ourselves to a few highlights which illustrate the performance of the instrument. The vignetting function (Figure 10) has been derived from a model validated by several independent observations. The difficulties here have resulted from unwanted reflections from the heat rejection mirror and the mirror-polished front face of the external occulter preventing the direct derivation of the vignetting pattern from the observation of a diffuse source. Note that the pylon which supports the external occulter does not block the field-of-view but distorts the otherwise axisymmetric pattern. The turnover of the vignetting function in the four corners of the image is due to the slightly undersized diameter of the polarizers.

Figure 12 presents the image of a grid placed at the focus of a collimator, the distance between the wires amounting to 135 arc-sec. The raw image has been fully reduced including the vignetting effect. Note that the full image has been recovered including the part behind the external occulter. The polarization state of the instrument has been characterized by the determination of the three most important terms of its Mueller matrix M_{11}, M_{12} and M_{13}. Each term is represented by an image giving the corresponding values at each pixel. Figure 13 gives the diametrical profiles of the three terms for the three polarizers oriented at 0°, -60° and +60°.

The measurement of the residual straylight in an externally occulted coronagraph is a most difficult, if not impossible, task. The results presented in Figure 13 have been obtained in vacuum with the NRL Sun-simulator. The heat rejection mirror was covered by a highly absorbing black lid to prevent the reflected solar light from flooding the wall of the vacuum tank. The straylight is composed of two distinct components, the defocused residual wing of the diffraction fringe from the external occulter which is not blocked by the inner occulter and a diffuse background which is essentially flat. As the laboratory set-up (even in vacuum) did not truly simulate the observational conditions in space, the present result may not be totally representative of the ultimate performances of C2. For instance, a careful examination of the diffuse background reveals that low contrast features of the vacuum tank (louvers) are detected which indicates that it is not strictly straylight. The experimentally measured straylight, in unit of solar radiance, has been compared with vignetted models of the corona (K+F). Figure 14 indicates that the corona will be easily detected down to 2.2 $R_\odot$.

7. The C3 Coronagraph

C3 observes the corona from 3.7 to 30 $R_\odot$. The 3.7 $R_\odot$ inner limit comfortably overlaps the 6 $R_\odot$ outer field limit of coronagraph C2. In common with coronagraph C2, the C3 instrument is an externally occulted coronagraph of a type successfully flown in orbit, and whose general characteristics have been described elsewhere (Koomen *et al.* 1975). However C3 has several features that are dictated by a small available space and by the especially large field limit of 30 $R_\odot$ (± 8°).

7.1. Design of C3

The C3 optical system is assembled into a three-part tube (Figs. 15 and 16) and installed in the LASCO instrument box, together with a triple mechanism (color filter and polarizer wheels and shutter) and CCD detector. The tube is then coaligned with coronagraphs C1 and C2 which occupy other sections of the box. At the top of the tube (Figure 16), a 110 mm diameter opening (A0) contains a centered occulting disk which shadows the small

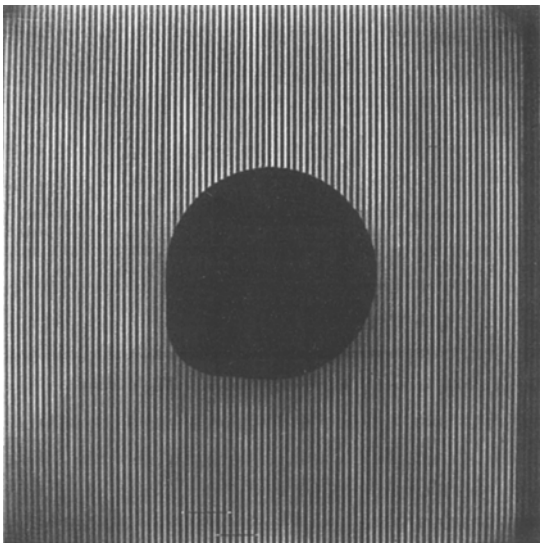

Fig. 12. Processed image of a resolution chart obtained with C2. The wire distance is 135 arc-sec.

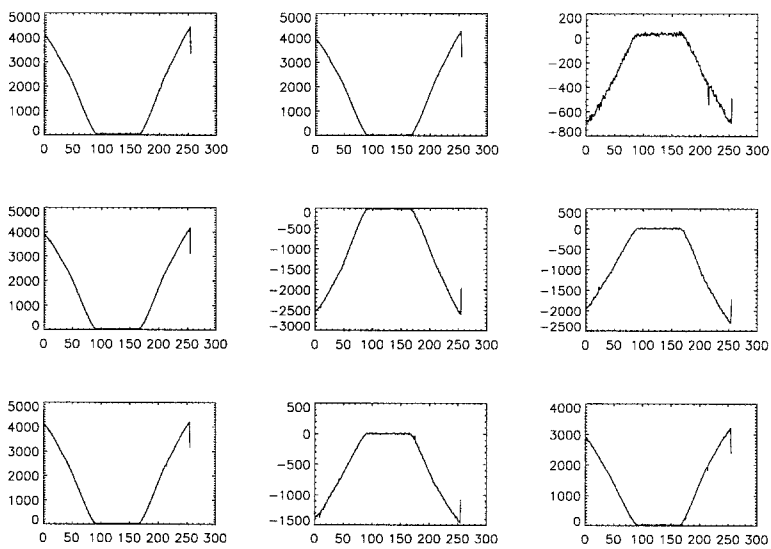

Fig. 13. Diametrical profiles of the images representing the M11 (first column), M12 (second column) and M13 (third column) terms of the Mueller matrix characterizing the instrumental polarization of C2

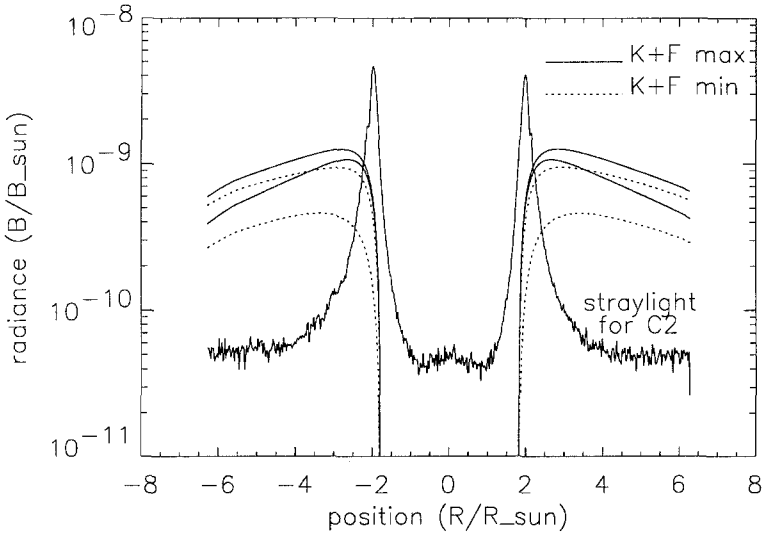

Fig. 14. Diametrical profile of the straylight obtained in vacuum with the NRL solar simulator together with equatorial and polar profiles of the K+F corona of the maximum and minimum types.

Fig. 15. The C3 instrument tube.

(9.6 mm) coronagraph aperture (A1) from all direct sunlight. The occulting disk is actually an assembly of three circular disks on a common spindle,

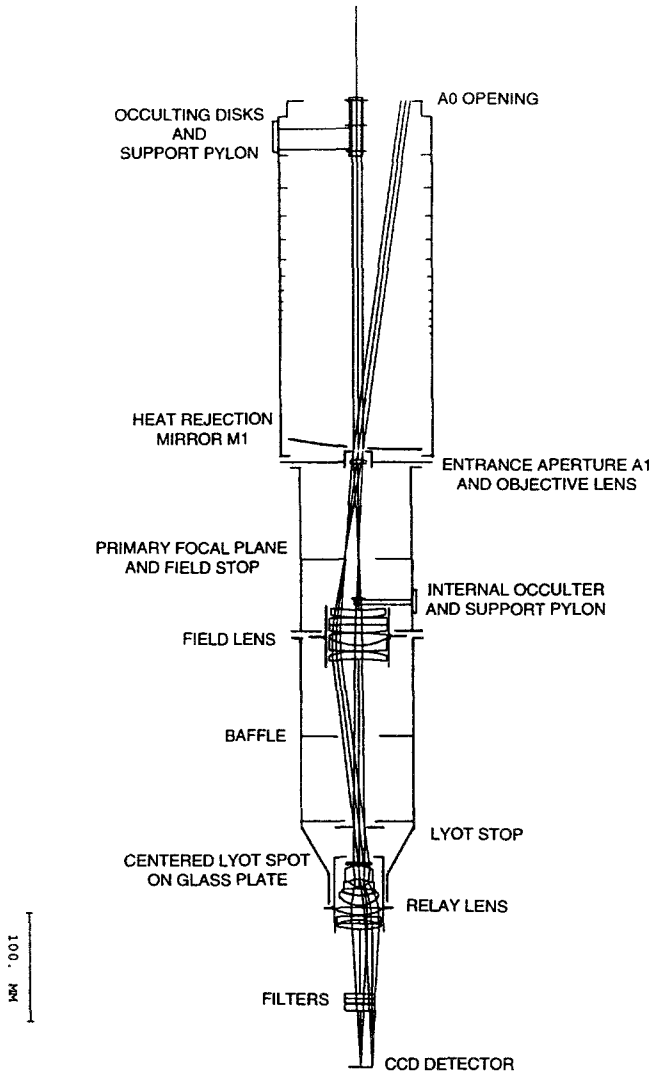

Fig. 16. The optical system and instrument tube of the C3 wide field coronagraph. A 30 $R_\odot$ and an axial (occulted) ray bundle are shown.

configured to minimize the diffracted sunlight falling on the A1 aperture and upon the objective lens which forms the primary image of the occulted corona. This image is followed by a central stop (the 'internal occulter') which intercepts the image of the external occulter and its halo of diffracted sunlight. Its supporting pylon intercepts light from the external pylon. Behind this stop is a large multi-element antireflection coated field lens which works at high relative aperture to present a nearly collimated coronal image to

TABLE V
System Parameters for C3

Overall length, entrance window to focal plane	889 mm
Effective focal length	77.6 mm
Field of view	circular
	occulted limit 3.7 $R_\odot$
	outer limit 30 $R_\odot$
Effective f-number	f/9.3
Resolution	58 arc sec per pixel
Corona unvignetted beyond 10 $R_\odot$	
Stray light	1×10^{-12} $B_\odot$

the relay lens. The field lens also projects a sharp image of the instrument aperture A1 upon the Lyot stop (A2), a circular aperture to intercept the remaining diffracted sunlight that originates at the A1 aperture edge.

The elements of the relay lens have been placed entirely behind this stop, to minimize the amount of diffracted light falling upon lens surfaces. All surfaces are anti-reflection coated. Altogether this lens is well suited to projecting a small coronal image upon the focal plane CCD detector, free of the stray light that has been removed by the upstream stops and apertures. Because of the presence of filter wheels before the focal plane, the relay lens must produce the small coronal image at a long back-focal distance, and it must also correct the aberrations carried through from the singlet objective lens. These requirements demand a many-element lens having the qualities of an inverted telephoto, with the Lyot stop near the telecentric position.

Because of the relatively short distance between the external occulting disks and the (A1) aperture, the coronal image is strongly vignetted, in the sense opposite to that of an ordinary camera, i.e., the bright inner corona is attenuated and suffers some loss of resolution. A compensating advantage is that the brightness range on the focal plane is reduced, so that the entire corona can be well recorded in a single exposure. The corona becomes unvignetted beyond 10 $R_\odot$. Some system parameters are give in Table V. The color filters for the C2 and C3 coronagraphs are shown in Table VI.

7.2. Suppression of Stray Light in C3

The C3 coronagraph is designed to observe the white light corona and zodiacal light to 30 $R_\odot$, where the brightness is about 2×10^{-11} of the solar disk. The stray light level of the instrument must be correspondingly low. In the externally occulted coronagraph the largest single source of stray light is the ring of diffracted sunlight from the edge of the external occulting disk. Some

TABLE VI
Color Filters for C2 and C3

Filter	Coronagraph	Nominal Bandpass (nm)
Blue	C2 and C3	420 - 520
Orange	C2 and C3	540 - 640
Light Red	C2	620 - 780
Deep Red	C2 and C3	730 - 835
Hα	C2 and C3	2.0 nm at 656.3 nm
Infrared	C3	860 - 1050
Clear	C3	400 - 850
3 Polarizers at 0°,±60°	C2 and C3	400 - 850

of this light is directed into the geometrical shadow of the disk and illuminates the A1 aperture and the objective lens. This illumination is reduced by adding two more disks on a common spindle, where each disk intercepts diffracted light from the edge of the one before. All disks are beveled to produce a sharp (.025 mm radius) edge which is polished and kept free of dust particles to minimize the quantity of scattered light entering the system. In addition, the internal image of the third disk is intercepted by a central stop to prevent the residual light from reaching the focal plane. This internal occulter is provided with a glossy black surface and is beveled to direct the light toward the outer walls of the instrument.

The entrance opening A0, which surrounds the external occulting disks, is also in direct sunlight and is provided with smooth-edged serrations to direct diffracted light away from the small objective lens aperture. The out-of-focus image of this opening is intercepted by an internal baffle which also acts as a field stop.

Of remaining importance is re-diffracted light from the edge of the objective aperture (A1) and scatter from the objective lens itself, since these are illuminated by residual light from the external disks. The lens is therefore a thin singlet of the clearest glass available to minimize volume scattering and is superpolished to minimize surface scattering. For this latter reason it is free of an anti-reflection coating. A smooth clean aperture edge and cleanliness of the lens surface must be maintained because a few large dust particles can neutralize the advantages of superpolish and glass clarity.

One consequence of the uncoated objective is a small ghost image of the external occulter, caused by inter-reflections between the two glass surfaces. This light is propagated down the system and re-imaged near the relay lens, where it is intercepted by the Lyot spot cemented to a glass plate at the front of the relay lens.

Among other sources of instrumental light is the tilted concave heat rejection mirror (M1). This mirror surrounds the small objective aperture (A1, Figure 16) and forms a small solar image that is reflected outward into the space between the occulting disks and the edge of the entrance opening (A0). Since the mirror is in direct sunlight, scattering from its surface can easily produce an unwanted illumination upon the tube baffles and upon the rear of the third occulting disk. This aluminum alloy mirror is therefore coated with electrodeless nickel, superpolished, and overcoated with aluminum and SiO_2 to provide a durable, highly reflective surface with minimum scatter.

A further attempt at light-reduction is made by using a large-diameter occulting disk spindle that is hollow over most of its length, with the open end directed toward the objective aperture (A1). The objective aperture therefore sees a large dark cavity centered in the third occulting disk.

All the instrument components including the entrance window are assembled and aligned in a tubular structure (Figure 15) and centered baffles are placed at intervals so that the objective, field and relay lenses see only the rear surfaces of baffles, or only the walls shadowed by preceding baffles. All parts are aluminum alloy, anodized and dyed a dense black. A long vacuum bake cycle is used to drive off any materials that may otherwise condense as light-scattering films upon the optics.

Of the light-reducing items mentioned above, the degree of occulting most strongly affects the final level of stray light, and is the parameter most easily changed by the experimenter. Increasing the diameter of the external occulting disks sharply reduces the stray light. Decreasing the diameter of the objective aperture, to bring its edge deeper into the umbra of the external occulter, has the same effect. At the conjugate positions to these items, increasing the diameter of the internal occulter or decreasing the diameter of the Lyot stop have a similar but more subtle effect. It is mostly a matter of trial and error to find a combination of these parameters to produce the desired level of stray light while occulting the Sun and inner corona as little as possible.

Considerable over-occulting of the Sun and inner corona was necessary to achieve the desired level of stray light over the coronagraph field. The practical minimum seemed to be an occultation to 3.7 $R_\odot$ to achieve a level of 10^{-12} $B_\odot$. It is very difficult to measure accurately a very low level of stray light because of the impossibility of reproducing a well-collimated 'Sun' surrounded by the black sky of in-orbit conditions. In the laboratory a particularly troublesome source of 'false' stray light was the instrument heat-rejection mirror, which reflected light from the test source back into the object space. Our best measurements were made in a long cylindrical tank, carefully baffled and blackened inside and evacuated to eliminate air scatter. The strong reflection from the heat rejection mirror was captured

as well as possible. The measured value of 10^{-12} $B_\odot$ is hopefully an upper limit.

Jackson and Lones (1994) have used the Breault APART scattered light software code to determine a theoretical stray light level for the C3 coronagraph, using the instrument parameters (apertures, occulting disks, baffles, walls, etc.). This study suggested that diffracted sunlight had been suppressed to the level where the stray light was determined only by reflective paths from light baffles and instrument walls. The computed level was not more than 2×10^{-13} $B_\odot$, considerably less than the experimental 'best measurement' of 1×10^{-12} $B_\odot$. It should be emphasized that application of the APART code is not simple, and that results depend on approximations of some instrument parameters as well as upon the number and nature of the light paths chosen.

Altogether, the experimental and computed values indicate that events in the faint corona to elongations as far as 30 $R_\odot$ can be observed without serious contamination by stray light.

8. Coalignment of C1, C2 and C3

The three coronagraphs are installed in a single rectangular instrument case $339.5\times323\times1362$ mm. The box was designed so that each experiment group could install and test its own instrument without interference from the other two groups and so that the finally assembled instrument case contained three coronagraphs whose solar pointing axes were aligned to 30 arc-sec.

To meet these two requirements the case is divided lengthwise into two equal halves, with each half precision-milled from a single block of aluminum tooling plate. The box was chemically cleaned to reduce the risk of residual contamination of the optical components. It was black anodized to satisfy the stray light rejection criteria. Finally, it was extensively vacuum baked to drive off residual contaminants which may otherwise condense as light scattering films on the optics. Box walls consist of a system of diagonal ribs with bosses as needed for lens mounts and other fixtures, and with a thin 1.5 mm membrane elsewhere. The box halves are joined via precisely milled flanges and dowels to form a single structure of maximum stiffness and minimum weight. Total weight of the box alone is about 21 kg. Internal partitions, which served to isolate one optical system from another, provide added stiffness.

One of the halves of the case is devoted to the C1 reflecting coronagraph, while the other half contains C2 and C3. For alignment and coalignment purposes each half is provided with a permanent optical boresight with an illuminated reticle. Each boresight was then aligned precisely to the long axis of the box, using the appropriate fixtures, alignment telescopes, lasers,

etc. The C1 and C2 optical systems were then installed and aligned in their respective box halves, using the boresight as the pointing reference.

The C3 coronagraph was assembled independently in its own tubular structure and later mounted alongside the C2 coronagraph. Tip and tilt adjustments are provided in the tube mounts to permit coalignment with the C2 coronagraph and boresight. It is of interest to note that determining the actual pointing direction of each coronagraph is remarkably simple. For example, an alignment telescope pointed into the C1 entrance aperture sees the collimated hole (the internal occulter) in the M2 mirror. This defines the Sun centered pointing direction completely, and it can easily be referenced to the boresight.

Similarly, the Sun-pointing directions of the externally occulted coronagraphs C2 and C3 is completely defined by the spindle which holds the occulting disks, which in turn cast a centered shadow upon the coronagraph entrance aperture. In the case of C2 it is the occulting cone which defines this axis. These axes can be optically compared with that of the boresight. After final assembly of the two halves of the instrument case our measurements indicate that the three coronagraphs are coaligned to within 60 arc-sec.

9. Detectors

9.1. CCDs

Each of the LASCO telescopes uses a three-phase, front-side illuminated, 1024×1024 pixel CCD manufactured by Tektronix to record visible light images of the solar corona. Each pixel is a square, 21μ on a side. There are four readout ports, one at each of the corners of the imaging area. Only one port is used at any time. The quantum efficiency of the CCD is about 0.3-0.5 in the 500 to 700 nm spectral region. The device is operated in the multi-phase-pinned (MPP) mode. While the MPP mode reduces the full well, it keeps thermally generated noise (dark current) to a minimum. The noise immunity of the MPP implant also helps to avoid the effects of noise generated by energetic particle radiation.

The flight candidate CCDs have very few defects. There are no column defects and less than 10 hot or dark pixels over the entire array. Since the full well capacity is slightly more than about 150,000 electrons, and the read noise of the output amplifier is greater than 5 electrons, a dynamic range exceeding 30,000 would have been possible. However, the quantization step has been set at about 15-20 electrons to match the capability of the analog-to-digital converter. Both vertical and horizontal charge transfer efficiencies (CTE) are better than 0.999999 for signal levels greater than 0.1 of full well. At low signal levels (0.01 of full well), the CTE drops to about 0.999995. The CCD will be operated at a temperature on the order of -80 C. Since

exposure times will be on the order of a few minutes, the dark current will be negligible.

The CCD is mounted on a custom multi-layer ceramic package that satisfies several requirements. The optical focal plane must be located very accurately in all dimensions. Dowel pin holes were provided in the copper-tungsten frame to accurately position the CCD to a known position and then to reposition it again if it were removed. The position of the CCD surface was measured optically, enabling a custom mounting plate to be made to accurately position the CCD focal plane to the optical axis to within 0.050 mm. The multi-layer ceramic package contains two integral heaters of different wattages. The low wattage heater is used to control the temperature of the CCD to within 2 C. The high wattage heater is used to raise the temperature of the CCD above the ambient to drive off any condensed vapors that might have collected on the surface. Temperature sensors are integrated onto the package and another on the CCD die itself.

The package has provisions for a non-flight cover to be attached over the sensitive CCD surface. The cover protected the surface of the CCD during handling. The cover shorts all of the pins to a large ground plane in the package to protect against damage caused by electrostatic discharge, a common failure mechanism for CCDs. This grounding cover remained in place until after the CCD was installed into the camera circuitry, after which the risk of discharge damage is minimal. The cover also provides a mechanical barrier to keep dust from collecting on the surface.

9.2. Cameras

The CCD camera was designed to be very conservative in power and mass cost. It uses about 5 W of power and weighs about 3 kg. In order to keep the CCD free from both chemical and dust contamination, the camera consists of two compartments. One compartment houses the CCD with a small opening for the incident beam and the second houses the camera electronics. The camera electronics has a vent path directly to the box exterior to avoid venting any contaminants into the optics compartment. The signals between the electronics and the CCD pass through a hermetic connector in the compartment wall.

The CCDs are cooled by passively radiating heat to deep space. A temperature of -80 C reduces the effects of permanent proton radiation damage to the bulk silicon, which causes a drastic drop in the ability of the CCD to transfer charge. For example, if the CTE is reduced to 0.999 the effect is such that the photoelectron charge packet for a point in the center of the array would be reduced by 64%, compared to only 0.1% for the undamaged CCD. At this CTE level, the image quality is virtually destroyed. Damage of this order could be caused by 3 or 4 large proton flares. Providing a mechanical shield of reasonable thickness would only reduce the CTE loss by a factor of

about 3-6, which is insufficient. In contrast, cooling to below -70 C can avoid almost completely the CTE damage produced by radiation effects. The low temperature slows the rate at which electron traps in the bulk silicon leak charge back into the image as the image is swept across the traps during readout.

The camera accepts 'high-level' commands to set up various parameters, to initiate the clearing cycle, and to initiate readout. The readout rate is 50,000 pixels s^{-1} so that it takes about 22 s for a full image readout including non-imaging pixels at the start and end of each line. The camera provides all of the clock signals and voltages required by the CCD and the analog signal processing chain. Among the setup parameters required are the beginning and ending pixels of the readout. This permits any arbitrary rectangle to be read out. Unwanted lines can be dumped at a rate of 0.060 ms per line. Thus any line on the CCD can be accessed within about 60 ms. Additional capabilities of the cameras include setting the number of cycles for clearing, setting slow or fast line dumping, selecting one of the four output ports, and setting voltages for radiation damage compensation.

The analog signal processing amplifies the output of the CCD by a factor of about 30, and uses double-correlated sampling technique to sample the photoelectron charge packet. The analog signal is digitized to 14 bits by an analog-to-digital converter, with a quantization step of about 15-20 electrons. The noise of the entire process has been measured to be about 25 electrons so that the dynamic range of the system is almost the full 14 bits, or about 16,000. Photon noise will be much higher than the noise in the measurement process.

The CCD is organized such that 20 non-imaging pixels at the beginning of every line are read out before the imaging area begins. The camera also reads out 50 pixels at the end of every line to ensure that the charge is completely cleared before the next line is transferred into the serial register. These non-imaging pixels can be used to calibrate various CCD characteristics such as charge transfer efficiency, read noise, and electrons per DN (digital number count).

10. LASCO Electronics and Instrument Control

10.1. Hardware Description

The LASCO and the Extreme Ultraviolet Imaging Telescope (EIT) experiments are both controlled by a single electronics unit, the LASCO Electronics Box (LEB). The LEB contains four types of cards: computer, random access memory, mechanism controller, and programmable-read-only-memory (PROM). The computer card contains two processors. One processor is the main LEB central processing unit (CPU). This is a radiation-hardened, 32-bit Sandia Lab SA3000 (15MHz clock), based on the National Semiconductor

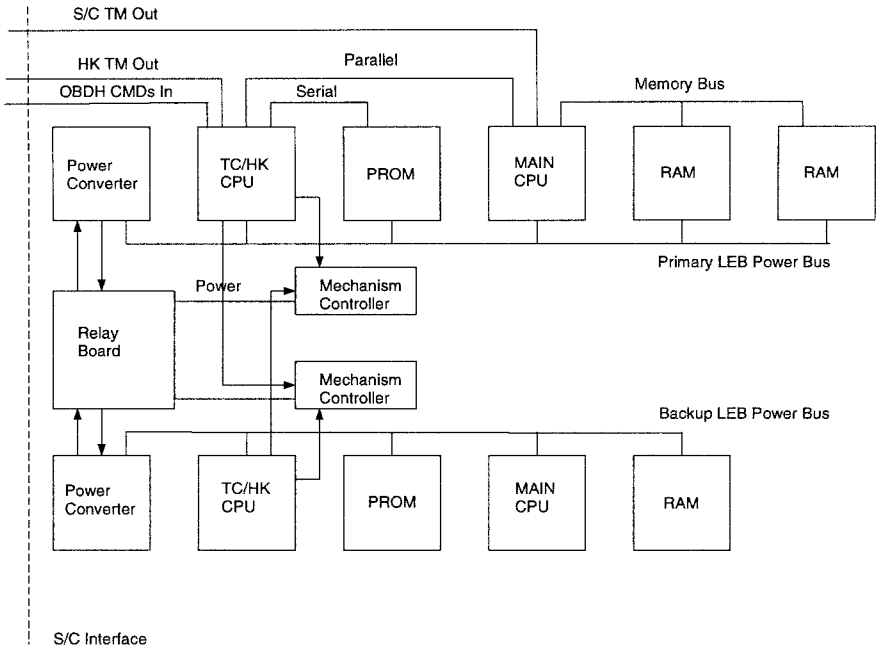

Fig. 17. A functional diagram of the LASCO electronics box (LEB).

32C016. The other processor on the computer card is an Intel 8031 which is integrated onto application-specific integrated circuits (ASIC). Other ASICs, which use the same Intel 8031 processor, are used to offload certain control tasks from the main CPU.

The LEB receives commands from the spacecraft, and provides science and housekeeping data to the spacecraft for telemetry. The command input and housekeeping telemetry are handled by the ASIC on the computer card. The science telemetry is handled by the Sandia CPU. The Sandia CPU also acts as the main controller for the electronics components of the experiment including the CCD cameras, the Fabry-Perot, telescope mechanisms such as shutters, filter wheels, and polarizer wheels, and the heaters and thermistors. Two mechanism controller modules provide redundancy. In addition, the LEB contains the power converters used to supply operating voltages to the LEB, the cameras, Fabry-Perot interferometer, pointing eyes, boresighter electronics, and M1 mirror controller.

The LEB has a primary and a redundant side (set of electronics) to increase system reliability. The selection of either the primary or redundant side is performed by ground command. The two sides have identical capability except for the amount of random access memory (RAM) - 12 Mbytes on the primary side and 6 Mbytes on the redundant side. The various subsystems, power converter, CPU, memory, PROM, and mechanism controller

are duplicated for the two sides. The interfaces to the spacecraft are also separate. The primary side of the LEB interfaces to the spacecraft primary side and the LEB redundant side interfaces to the spacecraft redundant side. The only cross-strapping is with the mechanism controller modules which allows either CPU subsystem to operate the mechanisms through either or both mechanism controller boards. This cross-strapping allows partial failures in the mechanism controllers to be overcome.

The LEB controls the experiment operations, manages the interface to the spacecraft computer, and performs image processing of the CCD camera data. In addition, it monitors the operation of the experiment and, via an analog-to-digital converter, provides measured values of voltages, temperatures, and other parameters to the experiment housekeeping data stream.

The CCD cameras contain their own processors but act as slaves to the LEB. They perform complex operations when commanded by the LEB, to reduce LEB processing requirements and to allow the LEB to efficiently perform as the overall operational coordinator. The communication link between the LEB and the cameras is via optically isolated, Manchester-encoded, serial channels. The three LASCO cameras and the EIT camera are all electronically identical. The EIT camera is unique only in its mechanical interface. Switched power is supplied to the cameras by the LEB and power returns from the cameras are brought back to the internal LEB single-point ground.

Similarly, the C1 Fabry-Perot interferometer contains its own processor acting as a slave to the LEB. Its primary function is to control the Fabry-Perot optical plate separation. It receives commands from the LEB, and provides status reports back to the LEB during operation. The communications link between the LEB and the Fabry-Perot processor is identical to the CCD camera link. The same command and data transfer protocol is used in both the camera and Fabry-Perot links. Power is also supplied to the Fabry-Perot processor and cameras in the same manner.

The programmable read-only-memory card contains one of the ASICs to control the operation of the two types of PROM that have been included. One type is bipolar PROM, which contains the software modules for all of the CPUs. Another type of PROM is electrically erasable (EEPROM), which can be altered after launch. This technology is not radiation-hard and will slowly degrade after launch. However, it will be acceptable during the initial post-launch checkout and will eliminate the need to upload large numbers of commands after any power outage. The length of time until the EEPROM fails is not exactly known, since the failure mechanism depends on the amount of time the EEPROM is powered. This time will be very short since it is powered only when the code is being transferred to RAM.

The LEB power converter subsystem provides the secondary voltages to all elements of the experiment except some spacecraft-powered heaters and thermistors.

There are 23 separate mechanisms in LASCO and EIT in addition to calibration lamps and paraffin actuators. For redundancy, there are two mechanism controllers but it is only possible to drive one mechanism motor at at time. This limits the power requirements to a reasonable peak value and allows for adequate power for individual motor operation. Each mechanism motor can be driven by either or both of the two mechanism controller modules in the LEB. Each mechanism has redundant encoders. The primary encoder set is connected to one mechanism controller and the other set to the other controller. Since either or both of the mechanism controllers can be powered-on at any given time, partial failures on either or both controllers can be overcome.

The LEB also provides thermal control of the five heater zones of the Coronagraph Optics Box (COB), and the two zones in the EIT. Thermal control of the COB is required to limit the lateral gradients which would tend to distort the telescope images. In the EIT, the two heater zones are used for focus control. Either instrument controller can drive a given zone heater, while each instrument controller reads its own set of redundant thermistors.

10.2. Software Description

The major functions of the flight software are command processing, instrument control, image processing and compression, status monitoring, and telemetry control. Each of the LEB processors has a small operating system (executive software) that understands a limited number of commands and performs a limited number of control tasks.

The Telecommand Executive (TCE) runs on the ASIC on the computer card and controls the telecommand and housekeeping functions. It receives commands from the spacecraft and forwards the command to the right processor. It queries the other processors for status and assembles the status into the packets for output to the spacecraft in the housekeeping packet data stream. It also monitors LEB voltages, currents, temperatures, Fabry-Perot temperatures and COB pointing to detect out-of-range conditions. Corrective actions are automatically taken to put the instrument into a safe configuration if safe limits are exceeded.

The Instrument Control Executive (ICE) runs on the ASIC on the mechanism controller card and controls the 23 telescope mechanism drivers, the calibration lamps and paraffin actuators. An additional function of the ICE is to control the five LASCO heater zones and two EIT heater zones by applying power to the zone heaters. A proportional-integral-derivative (PID) algorithm is used to perform the temperature control.

The PROM Card Executive (PCE) runs on one of the ASICs and controls the PROM card functions. The EEPROM will be used until a memory error is detected and then the bipolar PROM will be used. In addition, two copies of the PCE and TCE software have been written onto the EEPROM. These two copies are used during the initial boot process to avoid a single failure in the EEPROM. The PCE boot-strap software will try to boot PCE code off of the first copy and if that fails it will go to the second copy. The PCE then tries to read the TCE code from one of the copies in EEPROM. If that fails, the PCE will try to read the TCE code from bipolar PROM. On the next boot request, the PCE will try to read the TCE code from the other copy in EEPROM before reading the bipolar PROM.

The Observation Executive (OBE) is the software control program running on the Sandia CPU. It controls the communication with the cameras and Fabry-Perot interferometer and the output of data to the science telemetry stream. The OBE contains a number of software modules called LEB Programs (LP) to perform specific tasks. These tasks include loading the software into the peripheral devices (cameras and Fabry-Perot).

Many of the LPs control acquisition of an image or sequence of images from the telescopes. The entire procedure of collecting and processing an image is controlled by the LP. First the LP configures the telescope mechanisms, Fabry-Perot interferometer and M1 mirror drive (if necessary), and camera. Then it commands an exposure-readout cycle, including commanding the shutter to open and close as appropriate. The camera data is then transferred to the LEB, where it is compressed, formatted and passed to the telemetry system. LPs have been defined for calibration lamp images, dark current images and normal images, for example, to account for the different requirements on controlling the mechanisms and calibration lamps.

An LP can be scheduled to run immediately or at a future time. As part of the scheduling process, the LP duration must be specified. The duration can be either a number of iterations, a length of time or to run until an absolute time. There are four scheduling queues: dormant, wait, ready and current. All of the LPs are on the dormant queue at the start. When one of the LPs is scheduled by ground command to be run, it is transferred to the wait queue. When the time has been satisfied the LP is transferred to the ready queue. When the task on the current LP has completed, it is returned either to the ready, wait or dormant queue depending upon whether an additional instance of that LP has been scheduled. The highest priority task on the ready queue is transferred to the current queue and begins execution.

Normally, all of the LPs have the same priority. However, if a transient, for example, has been detected on-board, a set of observations to observe the transient would be put onto the ready queue at higher priority. Then when the current task has completed, the transient observing tasks would

begin execution. An example of a lower priority LP is the background task of peripheral status requests.

An LP can terminate normally as a result of either completing an iteration count or by exceeding the exit time. The LP will complete its current cycle and will terminate at a point that is appropriate for the LP. For example, an LP which takes several images per cycle will only terminate at the completion of the full cycle, not after one of the images in the cycle. However, this also implies that the next LP might not start at the expected time.

Since only one task can be on the current queue, only one LP can be operating at any given time. The LP must complete its cycle including transferring the compressed image to the output telemetry buffer. Observations can be interleaved, but this must be done by scheduling from the ground rather than by some sort of multiprocessing capability in the flight software.

Various instrument parameters such as exposure time, readout coordinates, etc., are specified through tables stored in RAM. The contents of the tables can be modified by ground command. These table content commands can also be scheduled much like an LP. This permits an observation to be made with one set of table entries, and then later the same LP can be performed with new table entries. There are three tables for exposure times: primary, alternate, and calibration. This distinction between the tables is meant for identification only, and each table is functionally the same. The primary and alternate tables provide the optimum exposure times for full field and reduced field readout, respectively. The calibration table provides the exposure times for calibrations using the internal lamps. The C1 Fabry-Perot interferometer exposure time table needs to have the exposure time for each wavelength step.

The memory available to an LP for image processing is any or all of the currently available memory. When the LP requests a section of memory to be allocated to it, one of five sizes of memory will be allocated to the LP, depending upon a memory management parameter. The three sizes correspond to a full image, a 1/4 size image (512×512), a 1/10 size image (256×400), a 1/16 size image (256×256), and a 1/64 size image (128×128). Once the LP has completed, the allocated memory returns to the available pool.

After taking, processing, and compressing an image, the data is passed to a 2 Mbyte image buffer. With the telemetry rate allocated to LASCO and EIT together (5.2 Kbs^{-1}), a full buffer will empty in about one hour. A goal of daily planning is to maintain data in the image buffer so that all of the available telemetry bandwidth is used.

10.3. Image Handling and Compression

The LASCO telemetry rate (4.2 Kbs^{-1}) would result in a transmission time of about 60 minutes for a full 1024×1024, 2 bytes-per-pixel image. Thus, image compression is desirable. A number of image processing techniques have been included in the flight software, from simple square root compression through transform encoding. The types of processing and compression utilized will be determined by ground command and executed through stored sequences with parameters stored in tables.

After a camera image is stored in a 2 Mbyte temporary image array, each image is logically blocked into 32×32 pixel blocks and assigned an absolute block number. This pixel block is the basic unit for transmitting images to the ground and the compression routines operate on the images one block at a time. The block numbering scheme is absolute and will be part of an image subheader returned to the ground. If a telemetry error occurs, resulting in the loss of a few telemetry packets, several entire blocks will be lost but subsequent blocks will be correctly located in the reconstructed image.

Two general classes of image compression techniques are included in the flight software. The first class consists of image processing techniques which, by themselves, do not directly compress an image but do transform the image into a format which is more suitable for true image compression. The second class are true image compression techniques which directly reduce the telemetry load. These consist of both geometrical techniques which reduce the total number of pixels composing an image, and coding techniques which reduce the number of bits necessary to transmit an image. Transform encoding yields the highest compression ratio but is very computationally intensive. Often a combination of geometrical compression followed by transform compression will be used. The trade off between temporal resolution and field coverage must be considered when observing programs are designed.

The following techniques prepare the image for true compression by transforming the original image into an new image whose intensity histogram distribution has more intensity values falling in fewer histogram bins than the original intensity histogram distribution.

DivideBy2: The image intensities are divided by 2. This can be repeated to obtain an even smaller range of intensities. This is equivalent to representing the intensities with one less bit for each division. This will be necessary when summing images together.

SquareRoot: The square root of the intensity is computed from a look up table. This reduces the number of bits required to represent the range of intensities by a factor of 2.

Difference: An image is subtracted from a second image taken at an earlier time and only the differences is transmitted. In a series of images, the second image can be either a constant image, or the immediately previous one. In

either case, original images can be reconstructed from differenced images on the ground. The potential compression factor depends upon the extent of variation between the two images. These variations are due to both photon noise and to coronal evolution.

Summed: The sum of a sequence of scaled images is transmitted. Since the intensity of an individual pixel in a camera image is represented by only 14 bits, there is potential headroom in the 16 bit output format to add together 4 original images. For more than 4 images it is possible to exceed the 16 bit limit. If the summed image is divided by a scale factor, this is avoided. This technique replaces a series of images by one image, and so can be considered a true compression technique, with the compression factor equal to the number of images in the sum.

10.4. Image Compression Techniques

The geometric data compression techniques for LASCO are:

Occulter: The image blocks (32x32 pixels) that are beyond the field limit or that are occulted by the occulting disk are not transmitted. Depending upon the telescope, the compression factor is between 1.3 and 1.5.

BadColAvg: Due to radiation damage, the CCD can develop a bad column in which the intensities in the column are saturated. This compression technique replaces the intensities in a bad column by the average of the neighboring (good) columns in order to achieve a higher compression factor. Uncorrected images may have a lower compression factor.

Mask: An arbitrary pattern can be transmitted by specifying a mask table of image blocks that are not to be transmitted. This can be used to transmit separate regions in the same image that cannot be represented by a simple rectangle. It can also be used to not transmit blocks containing bad (saturated) CCD pixels.

Subregion: Any rectangular subregion of the 1024×1024 CCD may be read out. This will be used to trade field coverage for time resolution. The only restriction is that the subregion must be a multiple of 32 pixels on a side and must begin at a pixel location which is divisible by 32.

PixSum: The LEB can form pixel sums (binning) of any rectangular array of pixels. This feature is also available on the CCD chip itself but is then limited to the dynamic range (14 bits) of the analog-to-digital converter.

RadialSpoke: An image is transformed into polar coordinates. In each 1° wide sector (pie shaped pieces), the averages along the 512 perpendicular chords are computed. Each of the 360 sectors is replaced by the 512 average values along a spoke through the center of the sector. This produces a compression factor of $1024 \times 1024/(360 \times 512) = 5.7$. An annular ring is then specified by an inner radius and an outer radius. By throwing out the pixels beyond the field limit or occulted by the occulting disk ('Geometric'), the compression factor becomes 6-9, depending upon the telescope.

InterMin: The goal of this function is to remove the effects of cosmic ray hits from an image. A cosmic ray will create a bright streak of photoionization electrons across the image. This function compares two images taken at different, but closely spaced, times and replaces pixels in the first image with those from the second image if the intensity value is lower.

The coding compression techniques can be divided into two categories, lossless or lossy, depending upon whether the reconstructed image is identical to the original image or not. The LASCO options are:

Rice: The Rice algorithm is a lossless scheme that creates a unique code for each intensity value that occurs in the image intensity histogram distribution. The code has a variable number of bits, depending upon the frequency of that intensity value, and the most frequent intensity is coded with the least number of bits. The Rice technique compares three different schemes for forming the unique code, and also a fourth uncompressed code. It then outputs the image using the most efficient coding scheme. The analysis is done in blocks of 32x32 pixels. The compression factor varies but is usually about 2.

ADCT: The Adaptive Discrete Cosine Transform is one of the most efficient transforms at compressing the information content into the fewest number of bits, although not all of the information in the original image is preserved (it is 'lossy'). The statistics of each image are examined to determine the coefficients of the cosine transform matrix which represents the image intensities with the least number of bits. Compression is achieved by then eliminating higher order coefficients according to the specified level of compression which can be as high as 100. Of course, the higher the compression factor, the higher the information losses. Compression factors higher than about 15-20 generally introduce unacceptable errors and will not be used on LASCO. The ADCT is computationally intensive, and the time needed to compress an image is independent of the degree of compression. The transform is performed on blocks of 32x32 pixels.

These compression schemes may be combined to achieve a higher compression factor. It is also possible to send down the same image processed in two different ways to test the effect of the compression. The average compression factor is expected to be about 10, which would allow one 1024×1024 compressed to be transmitted every 6 minutes for a total of about 240 images per day.

10.5. Description of the observing programs

The function of the LEB observing program (LP) is to coordinate the operation of the cameras, the Fabry-Perot, mechanism movements and the processing of the resulting camera images. A day's operation will be built up by scheduling various LPs to be performed. In order to meet the overall sci-

ence objectives it will be necessary to use many of the compression schemes described earlier.

Depending upon their function, the LPs have been classified into several categories: coronal imaging LPs, calibration LPs, status LPs, configuration LPs, and parameter table LPs.

10.5.1. Coronal Imaging LPs

This set of LPs obtain CCD images of coronal radiation. In all cases the tables defining the camera parameters, the exposure times, the method of image compression, and, in the case of C1, the Fabry-Perot wavelengths must be specified.

NORMAL: A single image is obtained with a specified telescope (C1, C2, C3, or EIT) at specified polarizer wheel and filter wheel positions. The camera parameter table and exposure time table are also specified. No commanding of the C1 Fabry-Perot (FP) is performed. Thus, this program would only be used for the C1 if the Fabry-Perot had already been commanded into the proper state, or if the image did not depend upon the Fabry-Perot configuration. The internal flow consists of telescope and camera setup, camera clearing, shutter open, expose, shutter close, image read out to the LEB, and compression and transfer to output buffer.

FP SCAN LINE: An image sequence is obtained with C1 at specified polarizer wheel and filter wheel positions using the Fabry-Perot at a sequence of wavelength positions to build a line profile. The internal flow consists of telescope and camera setup, FP setup, camera clearing, shutter open, expose, shutter close, image read out to the LEB, compression and transfer to the output buffer.

POLARIZATION SEQUENCE: A sequence of images is taken with a specified telescope at a single filter wheel position for a specified sequence of polarizer wheel position. Any of the five polarizer wheels positions may be used. The internal flow is the same as in the NORMAL program.

WOBBLE OUTSIDE: A dynamic imaging and Fabry-Perot sequence is taken with C1, in which FP SCAN LINE is performed at the four M1 mirror pointing positions. In a programming sense, two loops are performed, with the M1 mirror wobble as the outer loop and the Fabry-Perot scan as the inner loop. Dynamic imaging means that the M1 mirror is moved to the corners of a square, 2.8 arc sec (1/2 pixel) on a side. The internal flow consists of telescope and camera setup, M1 setup, FP setup, camera clearing, shutter open, expose, shutter close, image read out to the LEB, and compression and transfer to output buffer.

WOBBLE INSIDE: A dynamic imaging and Fabry-Perot sequence is taken with C1, in which an image is obtained at the four M1 mirror pointing positions for each wavelength step of the Fabry-Perot sequence. In a programming sense, two loops are performed, with the M1 mirror wobble as

the inner loop and the Fabry-Perot scan as the outer loop. Dynamic imaging means that the M1 mirror is moved to the corners of a square 2.8 arc sec (1/2 pixel) on a side. The internal flow consists of telescope and camera setup, FP setup, M1 setup, camera clearing, shutter open, expose, shutter close, image read out to the LEB, and compression and transfer to output buffer.

INTER SUM: A first image is taken from either C1, C2, C3, or EIT, and then a series of subsequent images, which are added or differenced from the first image. The intention is to improve signal-to-noise by averaging together a number of images. The filter and polarizer wheel can be moved to a different position for alternate images. No Fabry-Perot configuration is performed. The internal flow is the same as the NORMAL program.

SEQUENCE: Takes a sequence of images in any order of the telescopes (C1, C2, C3, EIT). If C1 is specified, a Fabry-Perot sequence is commanded. The internal flow is the same as NORMAL or FP SCAN LINE. This LP permits a pattern of observations to be repeated rather than explicitly scheduling the pattern. This will be very useful for the transient observing mode.

CONCURRENT: Takes a series of up to four exposures (one from each of the four telescopes) in which the start of the exposures is as closely spaced in time as possible. A table defines the offset times at which the various events in the camera exposure-readout cycle are to be performed, for each of the telescopes. These times are: when the camera is cleared, when the shutter is opened, when the shutter is closed, and when the camera readout and image processing begins. An image may be kept temporarily on one telescope camera CCD while an image from another telescope is being processed by the LEB.

10.5.2. Calibration LPs

The LPs that perform various calibration tasks are listed below. In all cases the tables defining the camera parameters, the exposure times, the method of compressing the image, and, in the case of C1, the Fabry-Perot wavelengths, must be specified.

DARK: A dark exposure is taken from a specified telescope. The shutter is not activated. The camera parameter table and exposure time are specified. The internal flow consists of camera setup, camera clearing, expose, image read out to the LEB, and compression and transfer to output buffer.

CAL LAMP: A calibration lamp exposure is taken for a specified polarizer wheel and filter wheel position. The camera parameter table and exposure time table are specified. The internal flow consists of telescope and camera setup, camera clearing, shutter open, calibration lamp on, expose, calibration lamp off, shutter close, image read out to the LEB, and compression and transfer to output buffer.

CONTINUOUS: An exposure is taken from a specified telescope (C1, C2, C3, or EIT), in the continuous readout mode, at a specified polarizer wheel and filter wheel position. The shutter is opened before the readout starts, and is closed after the readout stops. Thus, the CCD is exposed continuously during readout. The camera parameter table and exposure time table are specified. This continuous mode is generally used for calibration of the CCD readout system. The internal flow consists of telescope and camera setup, camera clearing, shutter open, image read out to the LEB, shutter close, and compression and transfer to output buffer.

CAM FP COORD: The Fabry-Perot subsystem performs several calibration tasks requiring a close coordination with the C1 camera. An adjustment of the Fabry-Perot plate separation or parallelism is made and the CCD is used to determine the transmitted intensity. The goal is to maximize the intensity. The types of tasks are finesse optimization, central aperture scan, and finesse measurement.

10.5.3. Status LPs

The LPs that determines the LASCO experiment status are as follows.

STATUS PERIPH: Request status from each of the peripherals. This LP is the default LP that is run whenever no other LP is running and so does not need to be explicitly scheduled by the ground.

STATUS M1: Request the M1 mirror drive measurement unit to sample the positional encoders for the M1 piezo-electric drives and the M1 temperature sensors.

STATUS MECH: Request status from each of the mechanisms. This enables an explicit request to obtain the true status of a mechanism at a particular time.

MEMORY DUMP: A section of memory from OBE, TCE, ICE or PCE can be dumped to the science channel. This LP is used only for debugging.

10.5.4. Configuration LPs

The LPs that perform subsystems configuration tasks are the following.

BOOT PERIPH: Load the camera or Fabry-Perot software into the peripheral. This is not normally used by the operator.

COMMAND PERIPH: Send a ground command directly to the peripheral. Camera and Fabry-Perot commanding are normally performed by the imaging LP. This would be used to set the peripheral into a particular mode that is not normally varied (such as camera readout port).

COMMAND M1: This LP provide a capability to either move the M1 piezo-electric drives to a new position. The WOBBLE LPs will provide M1 commanding in a specific sequence. This LP might be used to establish a new Sun-center position.

COMMAND MECH: Send a command to a mechanism. This would be used to schedule one of the mechanisms that are usually not commanded by an LP. The mechanisms that are not normally commanded are the doors, focus motors, C2 internal occulter disk assembly and the COB leg actuators.

10.5.5. Parameter Table LPs

The LPs that load the parameter tables are the following.

CAMERA DPT: This LP loads one of the three camera default parameter tables (primary, alternate, calibration) for a telescope to be modified. The camera DPT contains information related to the collecting of an image such as readout coordinates, on-chip summing, readout port, heater status, M1 lid status and shutter hold time. This LP then permits the DPT modification to be scheduled at an appropriate time during the day.

Acknowledgements

The LASCO instrument was constructed by a consortium of institutions: the Naval Research Laboratory (NRL, Washington, D.C. USA), the Department of Space Research, University of Birmingham (DSR, UK), the Max-Planck-Institut für Aeronomie (MPAe, Lindau, Germany) and the Laboratoire d'Astronomie Spatiale (LAS, Marseilles, France).

NRL is the lead institution in the consortium and was responsible for supplying the Fabry-Perot interferometer, the experiment electronics, the C3 coronagraph and the integration and testing of the experiment. The NRL effort was supported by NASA under NDPR S-92385-D. DSR was responsible for fabrication of the LASCO mechanical structure and providing the instrument pointing legs. MPAe was responsible for providing the C1 telescope, the instrument doors and the focus mechanisms. LAS was responsible for providing the C2 telescope, the filter wheel, the polarizer wheel and shutter mechanisms.

The following NRL personnel contributed significantly to the LASCO program: B. D. Au, G. E. Brueckner (principal investigator), D. J. Conroy, K. P. Dere, G. E. Holland, R. A. Howard (project scientist), M. J. Koomen, C. M. Korendyke, G. E. Kowalski (project manager),D. N. Lilley, N. R. Linder, W. L. Marlin, D. J. Michels (program scientist), J. W. Miller, N. E. Moulton, R. W. Moye, J. A. Oliver, N. C. Orrick, S. E. Paswaters, D. E. Roberts, R. E. Rubin, E. R. Simson, D. G. Socker, D. Wang, and R. S. Waymire.

Analytyx Electronics Systems Inc., Hudson, NH was responsible for the design, fabrication and test of the instrument electronics. Swales and Associates Inc., Beltsville, MD was responsible for the system engineering support, mechanical design of several optomechanical subassemblies and the thermal engineering effort. The LASCO instrument filters were produced

under the direction of B. Grenier and manufactured by the Andover Corp. (Salem, NH). The Fabry-Perot interferometer optical mirrors were provided by Queensgate Ltd. (UK). The C3 coronagraph optical system was designed at Tropel Inc., Fairport, N.Y. by G. K. Schnable and manufactured by that company. The instrument tube and mechanical parts were designed at Swales Associates, Beltsville, MD, by J. O'Connor and K. Kesarimangalam, with support from E. Devine and E. Smigocki. The C3 heat rejection mirror was provided by Hyperfine Inc. (Boulder, CO).

The C1 design was developed by MPAe in collaboration with the Carl Zeiss Company (CZ) in Oberkochen, Germany. CZ also produced the super-polished mirrors and other optical elements in C1. The REOSC company in Ballainvilliers, France, manufactured the M3 mirrors. The mirror coating was performed by General Optics Inc., Moorpark, CA. The C1 instrument was assembled and tested at the facilities of the Lindau Instruments GmbH (LI) in Lindau, Germany. The front doors and their driving mechanisms for all four telescopes of LASCO and EIT were designed at MPAe and manufactured by the Kayser-Threde (KT) GmbH in Munich, Germany. KT was also responsible for development and manufacture of the M1 tilt mechanism. The focus mechanisms for C1 and C2 and the protective lid in C1 were developed and fabricated at LI. The German part of the C1 effort was supported under grant 010C88024 by the Bundesminister für Forschung und Technologie.

Major contributions to C1 were provided by MPAe personnel: R. Schwenn (C1 project scientist), P. Hemmerich (project engineer and manager), P. Daly, A. Epple, B. Inhester, H.-U. Keller, H.-G. Kellner, R. Kramm, W. Kuehne, B. Podlipnik, H. Rosenbauer, M. Sperling, U. Spilker, and various contractors: R. Roll (for LI), G. Seipp (for CZ), J. Doerr and S. Hofer (for KT), R. Geyl (for REOSC), and others.

The C2 design was entirely developed in-house at LAS. Stigma-Optique in Vitry- sur-Seine, France, produced the super-polished, optically-contacted coronagraphic doublet which was coated by PMS, Boulder, CO. Other optical components were produced by Secia in Manosque, France and were coated by Balzers, Lichenstein. The external occulter was manufactured by Sopelem in Dijon, France. All filter and polarizers wheels for C1, C2 and C3 were developed and fabricated at LAS. The French participation in the LASCO project was financially supported by the Centre National d'Etudes Spatiales and by the Centre National de la Recherche Scientifique.

Major contributions to C2 were provided by the following LAS personnel: P. Lamy (C2 project scientist), J. Raynard (project manager), J.-L. Boit, J.-C. Berges, J. Billardon, J.C. Blanc, L. Castinel, G. Claysen, C. Colin, F. Daddi, P. Giraud, L. Hill, J.-P. Lecann, J. Lemerrer, P. Levacher, P.-L. Liotard, G. Moreaux, J.-C. Morellini, G. Moullet, G. Rousset, N. Taranto and G. Waultier.

The coronagraph optical box, which formed the optical bench, the boresighters, the instrument pointing system and the spacecraft interface were provided by the University of Birmingham. The structural analysis was done by S.M. Mahmoud, and the detailed design was implemented by M.J.Deeley. The linear actuators were provided by Schaeffer Magnetics, Chatsworth, CA. Spark erosion milling of parts of the COB was carried out by Vickers Shipbuilding and Engineering, Ltd, Barrow-in-Furness, UK. The environmental qualification was done at British Aerospace, Stevenage, UK. Modal analysis was performed by SDRC Engineering Services, Hitchin, UK. This work was supported by the Science and Engineering Research Council in the United Kingdom.

Other major contributions were provided by the following DSR personnel: G.M. Simnett (Local project scientist and manager), P. Beasley, D.K. Bedford, J. Bryant, C.J. Eyles, J. Greaves, B. Guest, J.R.H. Herring, A.L. Jones, R.W. Parry, S.P. Plunkett, A.J. Roberts, D.C. Smith, P.M. Thompson and A.P. Willmore.

References

Evans, J. W.: 1948, *J.O.S.A.* **38**, 1083
Evans, J. W.: 1953, *The Sun, G. P. Kuiper ed.*, Univ. of Chicago Press, Chicago 635
Fang, Y., Lamy, P.L. and Llebaria, A.: 1994, *Astron. Astrophys.* , submitted
Jackson, B.V. and Lones, L.A.: 1994, private communication.
Grotrian, W.: 1934, *Z. Astrophys.* **28**, 124
Jacquinot, P.: 1954, *J. Opt. Soc. Amer.* **44**, 761
Koomen, M. J., Detwiler, C. R., Brueckner, G. E., Cooper, H.W. and Tousey, R.: 1975, *Appl. Opt.* **14**, 743
Lamy, P.L., Bout, M.V. and Maucherat, J.: 1994, , in preparation
Lyot, B.: 1930, *C.R. Acad. Sci. Paris* **191**, 834
MacQueen, R. M., Csoeke-Poeckh, A., Hildner, E., House, L., Reynolds, R., Stanger, A., Tepoel, H. and Wagner, W.: 1980, *Solar Phys.* **65**, 91
MacQueen, R. M., Gosling, J. T., Hildner, E., Munro, R. H., Poland, A. I., and Ross, C. L.: 1974, *Soc. Photo-Opt. Instrum. Eng.* **44**, 207
Newkirk, G., and Bohlin, J. D.: 1963, *Appl. Opt.* **2**, 131
Roesler, F.L.: 1974, *Methods of Experimental Physics* **116**, 248
Tousey, R.: 1965, *Ann. Astrophys.* **28**, 600